A Study of Some Atmospherically Important Reactions with U.V. Photoelectron Spectroscopy.

A Thesis Submitted to the University of Southampton for the degree of Master of Philosophy.

Santiago De Frutos Del Rio

Department of Chemistry
University of Southampton

September 2002

MEMORANDUM

This thesis is an account of original research performed by the author in the Chemistry Department, University of Southampton between October 2001 and September 2002. Where findings of other work have been used, due reference has been given.

Acknowledgements

My thanks go to Prof. J. M. Dyke and Dr. A. Morris for their supervision, encouragement and help throughout this work.

I would also like to thank Dr. I. Torres for introducing me to the project and practical teaching on the operation of the spectrometer. Thanks also go to the rest of the PES group for keeping me entertained throughout the last year.

Finally thanks are due to the EC Reactive Intermediates RTN Network and NERC for sponsoring this year of study and to my family and my girlfriend for supporting me.

University of Southampton

Abstract

Faculty of Science

Chemistry

Master in Philosophy

A Study of Some Atmospherically Important Reactions with U.V. Photoelectron Spectroscopy (PES).

By Santiago De Frutos Del Rio

A number of reactions relevant to atmospheric chemistry have been studied by photoelectron spectroscopy (PES) in this work.

PES studies of the Cl+DMS (dimethyl sulphide), Cl+DMDS (dimethyl disulphide), Cl_2+DMS and Cl_2+DMDS reactions were performed for different reaction times at low pressure (~1 x 10^{-2} mbar in the ionization cell) and 298 K. It was found that the reaction Cl_2+DMS proceeds through a 1:1 complex HCl: CH_3SCH_2Cl which decays later to CH_3SCH_2Cl+HCl; DMDS reacts with Cl_2 directly to form CH_3SCl with no complex formation.

Both atom-molecule reactions, DMS+Cl and DMDS+Cl proceed through two channels. For the DMS reaction the first channel is Cl + DMS → HCl + CH_3SCH_2. Further reaction of CH_3SCH_2 with Cl_2 gives HCl + CH_3 + HClCS (1a). The second channel is Cl + DMS → CH_3SCl + CH_3 (1b). For the Cl+DMDS reaction the first channel is Cl + DMDS → HCl + CH_3SSCH_2. Further reaction of CH_3SSCH_2 with Cl_2 gives HCl + HClCS + CH_3S (CH_3S is short-lived and it forms either CH_3SH on reaction with DMS, or CH_3Cl on reaction with Cl_2) (2a). The second channel is Cl + DMDS → CH_3SCl + CH_3S. In studying these reactions, chlorine atoms were produced from two different sources: $SiCl_4$ and Cl_2 microwave discharges.

The final reaction studied was ethylene plus ozone. The main product of this reaction is formaldehyde but the main interest in this reaction is the role of one of its intermediates, the Criegee intermediate (alkene peroxy radical). The observation of O_2 $a1\Delta_g$ from the reaction is consistent with the presence of the Criegee intermediate in its singlet state.

List of contents

List of Figures

List of tables

CHAPTER 1.
Introduction

- ***1.0 Relevance to Atmospheric Chemistry.***

DMS and DMDS are released into the atmosphere by decay of organic matter [1]; they are also produced artificially by industry. These sulfur carrying gases can be converted in the atmosphere to SO_2, SO_3, and H_2SO_4 by processes initiated by OH radicals in the presence of sunlight [2], [3]. The oxidation mechanism in the presence of atmospheric oxygen includes formation of the peroxy radical $CH_3SCH_2O_2$, which further oxidizes to the final products through a multistep process [2]-[10]. Cloud production may be initiated by an aerosol precursor from these oxidation processes, and may be of climatological significance [11], as shown in Figure 1.0. Clouds can prevent ultraviolet radiation from passing through the atmosphere and this gives rise to climate cooling and acid rain.

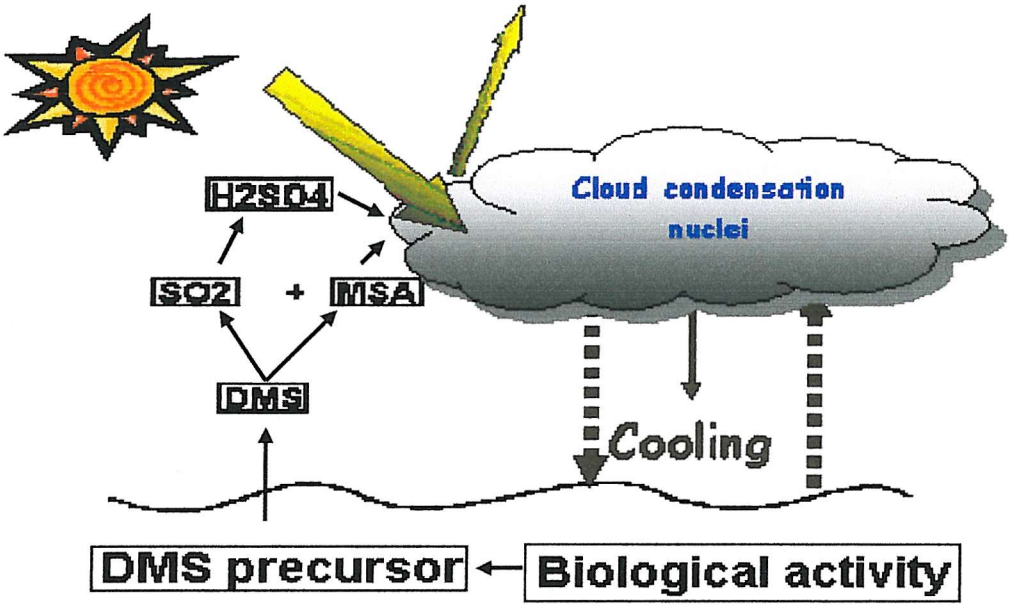

Figure 1.0: Schematic diagram of the impact of sulfur-containing compounds in the atmosphere. MSA = methyl sulfonic acid.

Chlorine compounds, such as chlorofluorocarbons, are released to the atmosphere by man and also molecular chlorine is formed under dark conditions by a heterogeneous reaction of ozone with sea salt in the presence of ferric ions

[12]. These compounds and molecular chlorine give rise to chlorine atoms in the stratosphere by photochemical decomposition, which give rise to destruction of the ozone layer. The reactions of these sulfur compounds with NO_3 radicals [10] and molecular chlorine during the night may also be significant. Though there have been no direct observations of the products of these primary steps as yet, kinetic studies have suggested that the major primary radical produced is CH_3SCH_2 from the Cl+ DMS reaction [2]-[10].

Kinetic studies have been carried out for reactions involving these sulfur-compounds using different techniques such as discharge-flow mass spectrometry [13], outdoor smog chamber experiments [2], time-resolved resonance fluorescence detection (RF) following laser flash photolysis (LFP) [14],[15], a quartz glass photoreactor with an FTIR facility [7] and a pulse radiolysis transient UV absorption spectrometer [8]. The most investigated reactions of DMS and DMDS are those with O, OH, Cl, Br, ClO, BrO and IO radicals of potential atmospheric relevance. Previous kinetic studies have been on the reactions of Cl/Cl_2 with DMS/DMDS [13] as well as on reactions of other halogens with DMS [16].

Despite intensive efforts both in laboratory and fields studies, there are still many uncertainties in the mechanism of DMS oxidation including identifying key intermediates and final products.

The reaction of ethylene with ozone is of great importance. The exact nature of the mechanism of the reaction is not properly understood. Ethylene and other alkenes are emitted from both anthropogenic and biogenic sources (e.g. forest trees) and are believed to react with ozone to produce OH which can react with DMS forming unwanted products. This reaction is a potential source of OH in the atmosphere at night.

The main aim of the present studies is to use PES to establish the mechanism of the reactions Cl+DMS, Cl+DMDS, Cl_2+DMS, Cl_2+DMDS and ozone+ethylene and this should help to establish whether these reaction routes can be important in the atmosphere.

- **1.1 References**

[1] S. F. Watts.
Atmospheric Environment 2000, **34**, 761-779.

[2] F. Yin, D. Grosjean, R. C. Flagan and J. H. Seinfeld.J.
Atmos. Chem. **11** (1990) 365-399.

[3] I. Barnes, K. H. Becker and I. Pastroescu.
Geophysical Research Letters **21**, No. 22 (1994) 2389-2392.

[4] A. J. Hynes, P. H. Wine and D. H. Semmes.
J. Phys. Chem. **90** (1986) 4148.

[5] E. P. Daykin and P. H. Wine.
Int. J. Chem. Kinet. **22** (1990) 1083.

[6] N. I. Butkovskaya and G. LeBras.
J. Phys. Chem. **98** (1994) 2582.

[7] I. Barnes, K. H. Becker and N. Mihalopoulos.
J. Atmos. Chem. **18** (1994) 267-289.

[8] T. J. Wallington, T. Ellermann and Ole J. Nielsen.
J. Phys. Chem. **97**, No. 32 (1993) 8442-8449.

[9] S. B. Barone, A. A. Turnippseed and A. R. Ravishankara.
Faraday Disscuss. **100** (1995) 34-54.

[10] C. Arsene, I. Barnes, K. Becker, R. Mocanu
Atmospheric Environment **35** (2001) 3769-3780.

[11] T. S. Bates, B. K. Lamb, A. Guenther, J. Dignon and R. E. Stoiber.
J. Atmos. Chem. **14** (1992) 315.

[12] Y. Sadanaga, J. Hirokawa and H. Akimoto.
Geophysical Research Letters **28**, No. 23 (2001) 4433-4436.

[13] N. I. Butkovskaya, G. Poulet and G. Lebras.
J. Phys. Chem. **99** (1995) 4536-4543.

[14] J. M. Nicovich, S. Wang and P. H. Wine.
Int. J. Chem. Kinet. **27** (1995)359-368.

[15] R. E. Stickel, J. M. Nicovich, S. Wang, Z. Zhao and P. H. Wine.
J. Phys. Chem. **96** (1992)9875-9883.

[16] J. Baker, V. A. Butcher, J. M. Dyke and E. P. F. Lee.
J. Phys. Chem. **99** (1995)10147-10158.

CHAPTER 2.
Experimental

2.0 Basic principles of PES

Since its development in the 1960s, photoelectron spectroscopy (PES) has proved invaluable as an experimental method which provides fundamental insight into the electronic structure of atoms and molecules.

When ultraviolet radiation of short wavelength interacts with free atoms or molecules, it can cause electrons to be ejected from the atomic or molecular orbitals. In 1887, Hertz discovered that irradiation of a solid alkali metal with ultraviolet radiation caused electrons to be ejected from the metal [1]. This effect was found only to occur when the frequency of the ultraviolet radiation was greater than a certain value; beyond this value the kinetic energy of the photoelectrons produced increased. In 1905, Hertz finding was rationalized by Einstein [2] who related the photon energy ($h\upsilon$), electron binding energy (I) and electron kinetic energy ($\frac{1}{2} m_e v^2$) by the energy conservation equation:

$$h\upsilon = \frac{1}{2} m_e v^2 + I \qquad (2.1)$$

Photoelectron spectroscopy is the study of these photoelectrons, whose energies, abundances and angular distributions are all characteristic of the individual atomic or molecular orbitals from which they originate. This method can be applied in the gas-phase or to solids and the two techniques are characterized by the type of radiation used.

X-ray photoelectron spectroscopy (XPS) applied to solid samples was developed in 1956 by Siegbahn [3]. X-ray radiation is sufficiently energetic to remove core electrons as well as valence electrons.

In the gas-phase, vacuum ultraviolet radiation was employed. The photons used have energies sufficient to ionize the valence electrons of atoms and molecules but not deeper lying core electrons. The technique, ultraviolet photoelectron spectroscopy, was developed independently by Turner and Vilesov [4, 5].

The photoionization process of a molecule, M, irradiated by a photon of energy, $h\upsilon$, to produce an ion, M^+, and a electron, e^-, may be represented in the following way:

$$M + h\upsilon \rightarrow M^+ + e^- \qquad (2.2)$$

In a photoelectron spectrometer, an intense beam of monochromatic (monoenergetic) ultraviolet radiation ionizes atoms or molecules of a gas in a ionization chamber. The photon source used is most commonly the helium resonance line (He I) at 584 Å (58.4 nm), which is equivalent to 21.22 electron volts (eV) of energy. This energy is sufficient to ionize electrons from the valence shell of atoms or molecules, that is, from orbitals that are involved in chemical bonding and are characterized by the highest principal quantum number of the occupied atomic orbitals. In each orbital of an atom or a molecule, the electrons have a characteristic binding energy, the minimum energy needed to eject them to infinity. Part of that energy of a photon is used to overcome this energy, I_n, and if the species is an atom the remainder, $h\upsilon - I_n$, must appear as kinetic energy (KE) of the ejected electrons:

$$KE = h\upsilon - I_n \qquad (2.3)$$

This is simply a re-arrangement of equation (2.1).

In a typical experiment, the ejected photoelectrons are separated according to their kinetic energies in an electron analyzer, detected and recorded. For an atom, the photoelectron spectrum is a record of the number of electrons detected at each energy, and contains a band at each energy, $h\upsilon - I_n$, corresponding to the binding energy, I_n, of each electron in the atom. If the species is a molecule, there are the additional possibilities of vibrational or rotational excitation on ionization, so applying the principle of the conservation of energy, the following expression for the kinetic energy of the photoelectron may be written:

$$E_{kinetic} = h\upsilon - I_n - \Delta E_{vib} - \Delta E_{rot} \qquad (2.4)$$

In equation 2.4, I_n, is the n_{th} ionization energy of the molecule (the difference between the energy of an ion and molecule in their ground rotational and vibrational states), and ΔE_{vib} is the change in vibrational energy occurring on ionization. The final term, ΔE_{rot}, is the change in rotational energy between M and M^+ on ionization and is included for completeness. It may be included in the term I_n as the typical resolution in vacuum ultraviolet PES is 250 cm^{-1} which is insufficient to resolve rotational structure. The vibrational spacing in a vibrationally resolved photoelectron band may be used to derive a value for the vibrational constant, w'_e, for the vibrational mode in the ion corresponding to the observed structure.

Two other quantities may be obtained from a photoelectron spectrum. The adiabatic ionization energy (AIE) of a photoelectron band is defined as the difference in energy between the neutral molecule in its ground vibrational state and the ground vibrational state in the ion. The ionization process may be represented as:

$$M\,(X,v''=0) + h\upsilon \rightarrow M^+\,(v'=0) + e^- \qquad (2.5)$$

The vertical ionization energy (VIE) is the difference in energy between the vibrational ground state of the molecule and the vibrational state, n, of the ion which has the highest overlap of its vibrational wavefunction with the v''=0 vibrational wavefunction. This ionization process may be represented as:

$$M\,(X,v''=0) + h\upsilon \rightarrow M^+\,(v'=n) + e^- \qquad (2.6)$$

The relative intensities of vibrational components in a photoelectron band are given by:

$$I_{v' \leftarrow v''} \;\alpha\; \left| \int \Psi' \Psi''\, d\,R \right|^2 \qquad (2.7)$$

where Ψ'' is the vibrational wavefunction in the initial neutral state and Ψ' is the vibrational wavefunction in the ion. This is considered in more detail in the next chapter.

The energy of the photoelectron bands and the relative intensities of the vibrational components within a band have been considered so far. The relative intensity of the bands themselves also give useful information, which is needed in order to be able to analyse the photoelectron spectra of molecules whose ionic states have not already been identified. The relative areas of photoelectron bands in a spectrum are approximately proportional to the relative probabilities of ionization to the different ionic states, but experimental factors are also involved. The relative ionization probabilities, called relative partial ionization cross-section, can be derived from the measured spectra. For vibrationally resolved bands, the intensity is obtained by summing the intensities of all the vibrational components.

The unique feature of ultraviolet PES is the ability to eject electrons from any of the occupied valence energy levels of a molecule. As each of these levels has its own energy, electrons from each level may be studied. In practice, for a closed-shell molecule, PES provides an experimental picture of the molecular orbital energy diagram of a molecule and may also provide an insight into the bonding character of the orbitals ionized [6,7].

Early photoelectron spectroscopic studies concentrated on gases and volatile liquids as it was easy to obtain a sufficient vapour pressure of the sample to produce a spectrum. Two areas which have been considered by the Southampton PES group are the PES study of short-lived species generated by rapid atom-molecule or molecule-molecule reactions, and the PES study of involatile compounds where photoelectron spectra have been obtained by increasing the vapour pressure of a solid by heating [8, 9]. This present work made use of the first kind of these studies to study some reactions of atmospheric relevance.

In order to assist the assignment of the photoelectron spectra obtained, ab initio molecular orbital calculations have been carried in the Southampton PES group.

• 2.1 Main parts of the Photoelectron Spectrometer.

- *2.1.1 The Single Detector Photoelectron Spectrometer.*

All the photoelectron experiments described in this work were carried out on a single detector photoelectron spectrometer, designed by Dr. Alan Morris of Southampton PES group, for the study of short-lived species in the gas-phase.

The basic requirements of a photoelectron spectrometer are:

- an ionizing radiation source,
- an ionization chamber,
- an electron energy analyzer, and
- an electron detector.

A schematic diagram of the apparatus used in this work is shown in figure 2.1. The whole apparatus must be evacuated to low pressure so that electrons produced by photoionization do not undergo inelastic collisions.

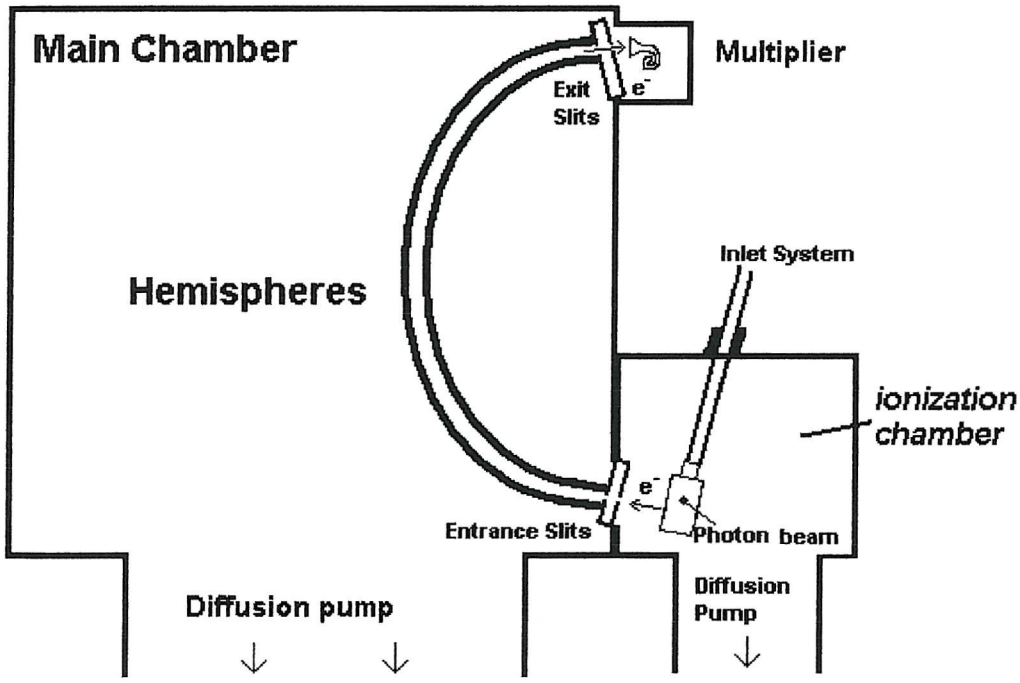

Figure 2.1: A schematic diagram of the photoelectron spectrometer used in this work.

In a photoelectron experiment sample gases are admitted into the ionization chamber through the inlet system. The gas is crossed by the ionizing radiation source resulting in the production of photoelectrons. A sample of these electrons is taken at 90° to the photon beam, by the entrance slits of the spectrometer, where they pass into a 150° hemispherical electrostatic analyser. This analyser separates the electrons according to their kinetic energy by voltages applied to the spheres; those which pass through are detected by a channeltron electron detector. To obtain a photoelectron spectrum, the voltage on the hemispheres (which are equal and opposite) are swept linearly and plot is made of intensity versus electron kinetic energy. The components of this apparatus and the main instrumental characteristics will now be described.

- *2.1.2 Ionizing Radiation Source [10, 11].*

The principal requirements of the radiation sources used in photoelectron spectroscopy are monochromaticity and intensity. The photon source should also be sufficiently energetic to remove valence electrons from molecules. The most efficient and intense ionizing sources have proved to be resonance lines produced in rare gas discharges. The most useful and widely used photon source in photoelectron spectroscopy is a discharge in pure helium, which gives the He I resonance line at 584 Å, corresponding to a photon energy of 21.22 eV. It is the most frequently used because of its ease of production, spectral purity and because it has the energy to ionize all the valence electrons from most molecules; the characteristics of such sources are well documented [10, 11]. This emission line occurs as a result of excitation of He from its $1s^2$ (^1S) ground state to the $1s^12p^1$ (^1P state) followed by emission.

The resulting decay, $^1S_0 \leftarrow {}^1P_1$, produces photons of energy 21.22 eV and this account for greater than 98% of the total emission. Higher members of this series, that is, 1s np...^1P (with n>2) to the ground state, are also present in the output of helium discharge lamps, but their intensity is not more than a few per cent of that of the 584 Å line. The lines of this series, starting from the 584 Å line,

are called He Iα, He Iβ, etc., and some of them are listed in Table 2.1. The work described in this thesis employed exclusively He I radiation.

Line	*Wavelength, Å*	*Energy, eV*	*Intensity*
He Iα	584.33	21.218	100
He Iβ	537.03	23.083	2
He Iγ	522.21	23.742	0.5
He IIα	303.78	40.814	<1
He IIβ	256.32	48.372	
He IIγ	243.03	51.017	
He IIδ	237.33	52.241	

Table 2.1: Lines from a helium discharge lamp. The relative intensities given are typical for a capillary discharge under normal operating conditions for He Iα output. The relative abundance of the lines of higher energy, notably He II lines, can be increased at low pressures.

The helium photon source used in this work is a low pressure discharge with differential pumping. A d.c. discharge was struck in helium gas flowing through a capillary placed between two stainless steel, water cooled, electrodes. The helium gas used was purified by passing through a liquid nitrogen cooled zeolite molecular sieve trap before entering the lamp. As the lamp is windowless, as vacuum ultraviolet radiation is easily absorbed by window materials due to its short wavelength, differential pumping was required to prevent helium gas entering the ionization chamber. In this manner, self-reversal [12], where He I radiation is absorbed by the ground state helium atoms in the photon beam path, is minimized. Self-reversal results in an increase in the effective linewidth of the radiation as the central core of the radiation is more highly absorbed than the "wings". This build up of intensity in the wings results in an increased linewidth; a photon energy spread of 2 meV is typical [12].

- 2.1.3 Magnetic Shielding [11, 13].

Electrons being light, charged particles are easily influenced by stray electric or magnetic fields. Ideally electrons produced in the ionization chamber should experience no stray fields, and the electrons which pass through the entrance slits should only experience the electrostatic field of the hemispherical analyser. For this reason, the components of the spectrometer are constructed from nonferromagnetic materials. Local charging effects on the internal surfaces of the spectrometer are minimized by coating the ionization chamber, entrance and exit slits and the hemispheres with colloidal graphite (DAG). This coating should be replaced after chemical contamination (for example after each experiment involving discharged chlorine). The modular nature of the spectrometer facilitates the cleaning and graphite coating process.

The components of the earth's magnetic field are counteracted by applied fields from currents passed through three pairs of mutually orthogonal Helmholtz coils. The currents passing through these coils are adjusted such that signal intensity is optimized. The He I photoelectron spectrum of argon is used for this purpose.

- *2.1.4 Vacuum System [11, 13].*

The spectrometer pressure required to analyse and detect photoelectrons from gaseous samples is dictated by the mean free path required for a photoelectron to pass from the point of ionization to the channeltron detector and by the operating pressure of the channeltron itself. Pressures below 1 x 10^{-4} Torr give mean free paths in excess of 1 meter and prevent arcing of the applied voltage (≈2.5 kV) on the channeltron.

The pumping system employed on the instrument used in this work consisted of two 9" (1300 ls^{-1}) oil diffusion pumps, each backed by a two stage rotary pump. These were used to pump the ionization and the analyser chambers respectively. A further rotary pump was employed to provide differential pumping for the helium lamp to prevent helium from the lamp reaching the ionization chamber. A third 6" diffusion pump backed by a two stage rotary pump was used to increase the pumping on the ionization chamber to reduce chemical contamination, specifically during experimental work involving chlorine. To further increase the pumping efficiency in the ionization region, the front diffusion pump is fitted with a liquid nitrogen trap. With this pumping system, the base pressure in the ionization and in the analyser regions is approximately 4 x 10^{-6} mbar with no added gases and typically ≈ 1 x 10^{-5} mbar with a sample gas added.

- *2.1.5 The Electron Energy Analyser [11, 13, 14].*

The requirements of an electron energy analyser are the separation of electrons according to their kinetic energy whilst maintaining high resolution and transmission. The analyser used in this work was a 150° hemispherical analyser. This reduced angle (from 180°) allows the entrance and exit slits of the spectrometer to be positioned in a plane, near the focal points of the analyser, whilst keeping the electron source, electron focus and the centre of the hemispheres on the same line. Photoelectrons are separated according to their kinetic energy by the application of equal and opposite, positive and negative voltages to the inner and outer hemispheres respectively. In this way only electrons of a certain kinetic energy can pass through the analyser for a given applied potential (V).

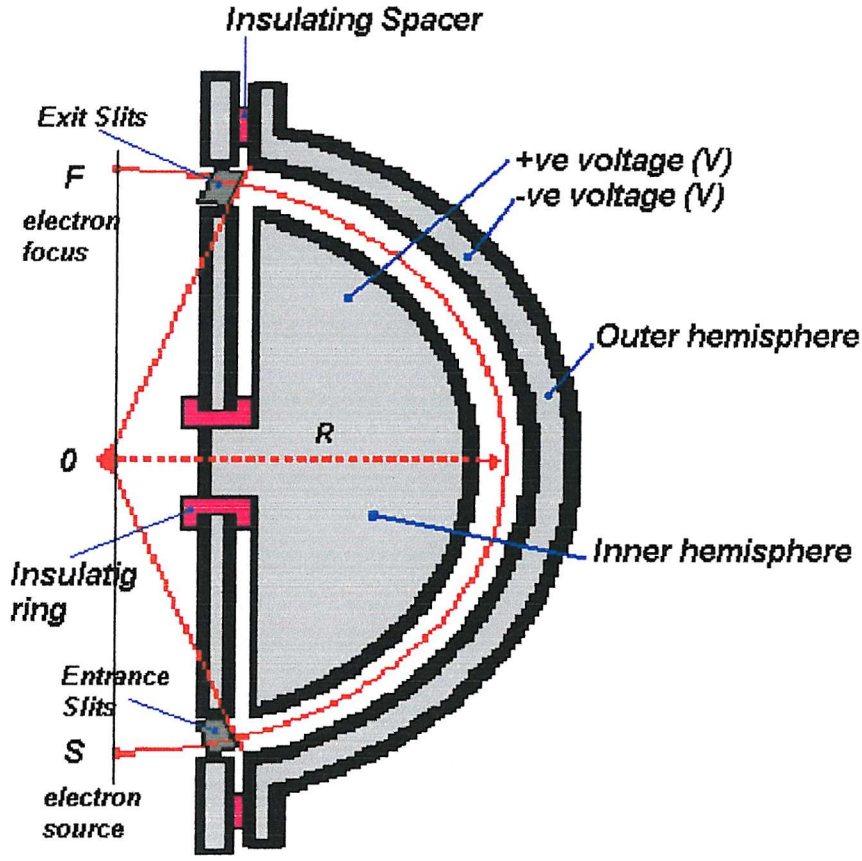

Figure 2.2: Schematic diagram of the electrostatic electron energy analyser used in this work.

As shown in Figure 2.2, photoelectrons which pass through the analyser are focused onto a channel electron detector. This detector consists of a layer of semiconducting material, possessing good secondary electron emission characteristics, deposited over the interior surfaces of a wound tube. A schematic diagram is shown in Figure 2.3. A potential difference of approximately 3 – 2.6 kV is applied between the ends of the channeltron establishing an electric field along its length which accelerates the secondary electrons produced. Electrons striking the channeltron surface cause a cascade of secondary electrons which produce a pulse in an external electrical circuit, with typical gains of the order 10^6 being obtained. The signal is passed through a preamplifier, amplifier, and then on to a ratemeter and a chart recorder. In order to make the work with the data easier, the conversion of the spectra into computer files was done by using a scanner and digitalization process.

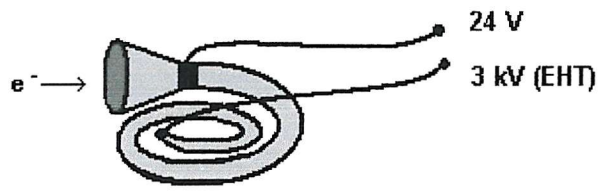

Figure 2.3: Schematic diagram of the channeltron electron detector used.

- *2.1.6 The reaction cell [15].*

In order to obtain an acceptable photoelectron signal intensity, a concentration of the species of interest of approximately 10^{10} molecules cm^{-3} in the ionization region is required. Many short-lived molecules may be formed in low partial pressures, on the threshold of detection by PES. This low partial pressures invariably results in poor signal to noise ratios in the photoelectron spectrum. By placing a cylindrical, brass cell of approximately 1 cm diameter coaxially with the photon beam in front of the entrance slits, the local pressure of a gas may be increased by a factor of 10-100 [15]. The reaction cell has two pairs of knife edges which are aligned with the entrance slits of the photoelectron spectrometer. The resulting higher effective pressure in the ionization region leads to an improved signal intensity. However there is a disadvantage associated with using a reaction cell. The tolerance of the instrument to chemical contamination is reduced, as local charges may build up close to the point of ionization, resulting in a loss of resolution and signal intensity. However, this varies with the sample used and the effect must be tested for each sample gas. The reaction cell used in this work is shown schematically in Figure 2.4:

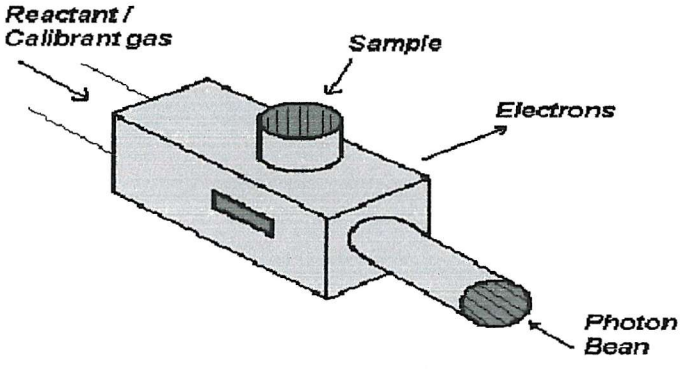

Figure 2.4: Schematic diagram of the reaction cell used in this work.

- *2.1.7 Instrumental Resolution.*

The resolution of the photoelectron spectrometer is defined as the full-width at half-maximum (FWHM) of the $(3p^{-1})$ Ar^+ $^2P_{3/2} \leftarrow$ Ar $^1S_0$ ionization. The standard operating resolution of the spectrometer used in this work was 30 – 35 meV. This base resolution is limited by several factors, of which the main factor is the ability of the electron energy analyser to discriminate between electrons of differing kinetic energy controlled by the slits width and the mean radius of the hemispheres [16]. Other small factors are the linewidth of the photon source, Doppler broadening and sharing of the momentum between the ion and the electron.

In practice, where the mass of the ion is greater than 20 a.m.u., the error resulting in assuming that the electron carries away all the liberated energy is very small ($\Delta E = m.E / M$, where m is the mass of an electron and M the mass of the ion); for electrons of kinetic energy 10 eV, the error would be < 1 meV.

The natural linewidth of He I radiation is approximately 2 meV and hence this is not a major contributor to the experimental base resolution as self-reversal mentioned previously is minimized through differential pumping. The contribution due to Doppler broadening [13] arising from thermal motion of the sample gas species may be estimated by assuming the most probable velocity of the target molecule to be given by:

$$v = (2kT/M)^{1/2} \qquad (2.7)$$

where v is the velocity corresponding to the maximum of the Maxwell distribution. It may be shown that [16] the width ΔE associated with Doppler broadening is:

$$\Delta E = 2(mEkT/M)^{1/2} \qquad (2.8)$$

For molecules of mass, M, 100 a.m.u, electrons of kinetic energy 10 eV and a temperature of 300 K, ΔE is approximately 0.004 eV. This effect is clearly of more importance for lighter molecules, for example molecular hydrogen, where

photoelectrons arising from He I ionization (of kinetic energy approximately 5 eV) have thermal widths of 0.02 eV.

However, the major factor in determining the base resolution of the instrument is the geometric characteristics of the electron kinetic analyser and slits. A schematic diagram of the electron analyser used in this work is shown in Figure 2.2. The source of this contribution to experimental resolution will be now considered.

An electron traveling around the hemispherical analyzer in an orbit of mean radius R will only maintain a stable orbital when the electrostatic and centripetal forces acting upon it are balanced. For a stable trajectory:

$$eF = (mv^2)/R \tag{2.9}$$

In this equation, e is the charge of an electron, F is the electric field between the hemispheres, m is the mass of an electron and v is the electron velocity. For a given electric field strength only those electrons of a certain kinetic energy may pass through the analyser. The kinetic energy, E, of the electron in a stable trajectory may be then be written as:

$$½\ mv^2 = ½\ eFR = E \tag{2.10}$$

If the photoelectrons entered and exited the analyser through point sources, the kinetic energy of the transmitted electrons would be known exactly. However in order to transmit a sufficient number of electrons the entrance and exit slits have to be of finite width, typically 1 mm. This means that a range of electron energies is allowed to pass through the analyser for a given electric field strength. It is this factor which results in the loss of base resolution. From the equation (2.10), the electron kinetic energy range (ΔE) accepted by the analyser is related to the orbit radius, R, and the electric field, F, by:

$$\Delta E = ½\ eF\ \Delta R \tag{2.11}$$

Therefore

$$\Delta E / E = \Delta R / R \qquad (2.12)$$

For a total slit width, S, R has a value of S/2 which results in:

$$\Delta E / E = S / 2R \qquad (2.13)$$

In this equation ΔE is the full width at the base of a photoelectron peak. For the band profiles obtained with the hemispherical analyser used in this work, equation (2.13) may be rewritten in terms of the width at half-height $\Delta E_{1/2}$ [17]:

$$\Delta E_{1/2} / E = S / 2R \times 1 / 2.3 \qquad (2.14)$$

For fixed entrance and exit slit widths, the resolution is proportional to electron kinetic energy. For example, the instrumental resolution for 5 eV kinetic energy electrons, passing through a total slit-width of 1 mm and traversing a hemispherical analyser of 10 cm radius, would be approximately 11 meV (half-height). A disadvantage of a hemispherical analyser in which the voltage difference on the hemispheres is swept to obtain a spectrum, is that the transmission of the electrons of different kinetic energies is not constant. It has been found that the transmission of electrons of kinetic energy in the range (1 – 10 eV) is linear and proportional to the kinetic energy [18], and the transmission of low kinetic energy electrons (<1 eV) is fairly poor. This problem may be overcome by applying an accelerating potential to the photoelectrons thus enhancing transmission of low kinetic energy electrons.

- 2.1.8 Inlet System.

From a photoelectron spectrum one is able to measure ionization energies of reactants, reaction intermediates and reaction products in a reaction mixture, which, in combination with appropriate electronic structure calculations can provide an identification tool for those species. In order to study intermediates and products of reactions to establish the mechanism of a reaction, the system used to introduce the reactants must allow the measurement of the spectra at different reaction times.

The inlet system used in this work consists of a glass tube, with a lateral outlet (in a "T" shape), Figure 2.5, with an inner glass tube which can be moved with respect to the ionization point. With this tube, one of the precursors is allowed into the system through the lateral outlet and the other one through the inner tube. Accurate calculations [19], taking into account the pumping efficiency, the average pressure in the tube and the molecular masses involved in the reaction, show that a mixing distance of 1 cm between the mixing and ionization points corresponds approximately to a reaction time of 0.5 ms.

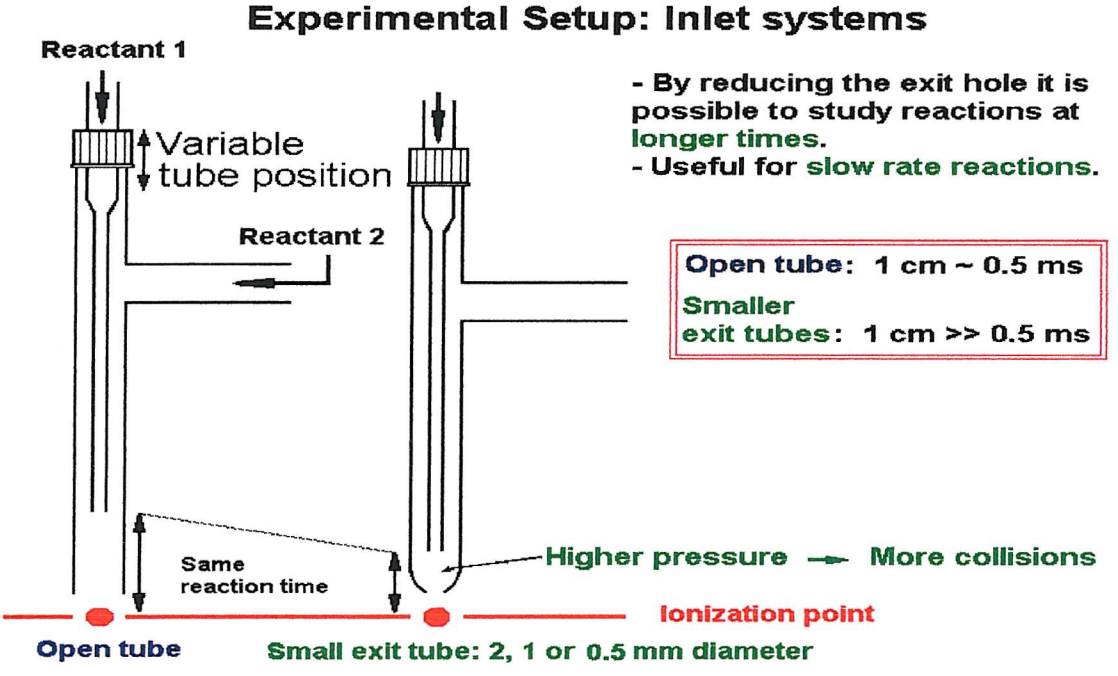

Figure 2.5: Schematic diagram of the inlet systems used in this work.

If the size of the exit hole is reduced as shown in Figure 2.5, the pressure in the system increases and more collisions occur. This means that for the same mixing distance the reaction time is longer for a smaller exit hole inlet system, so that in this case, slower reactions may be studied. Depending on the rate of the reaction being studied, either an open tube or one of several smaller exit tubes can be chosen.

- 2.1.9 Production of short-lived species.

As mentioned previously, in order to study a species by PES a concentration of order 10^{10} molecules cm^{-3} in the photon beam is required. In practice, this means that, with an open inlet system and with the pumping system used, an atom-molecule reaction with a rate constant of 10^{-11}-10^{-10} cm^3 $molecules^{-1}sec^{-1}$ is required. Most atom-molecule reactions are too slow to generate such a concentration of short-lived species. In this work, chlorine atoms are produced by a microwave discharge (2.45 GHz) of molecular chlorine or silicon tetrachloride (argon was used in the discharge as a carrier), and reacted with a chosen target molecule (DMS or DMDS) inside a boric acid coated Pyrex inlet tube. The microwave cavity was placed on the lateral outlet of the inlet system and connected to the microwave supply. A schematic diagram of the inlet system used in this work is shown in Figure 2.6. A study of the spectra recorded at different mixing distances allows the main reaction pathway to be determined.

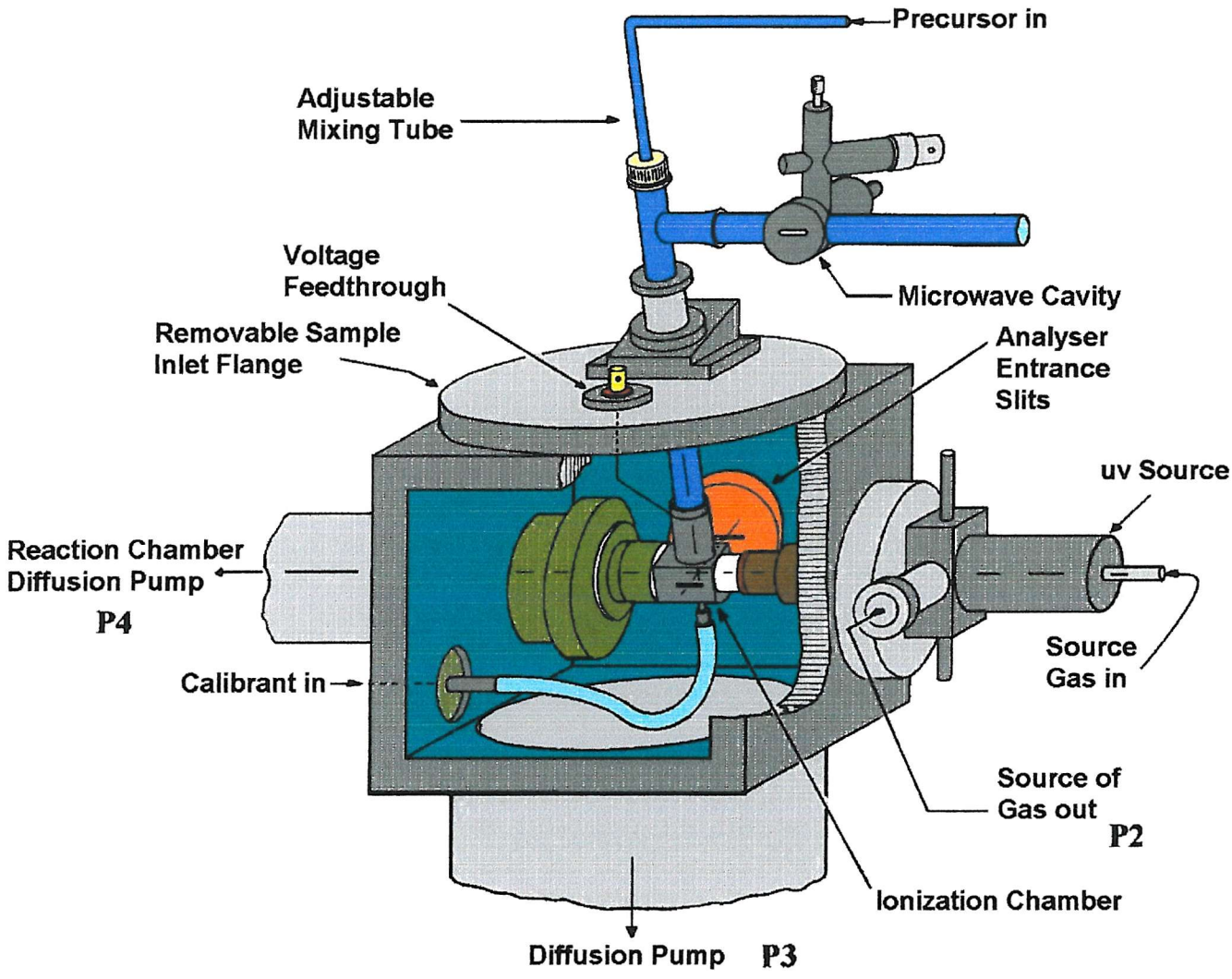

Figure 2.6: Schematic diagram of the spectrometer with the microwave cavity attached to the inlet system.

- 2.1.10 Long Inlet System.

For the study of one reaction (ozone + ethylene), a "new" inlet system has been designed to allow this reaction to be studied. This reaction is very slow having a rate constant at room temperature of 1.91×10^{-18} ($\pm 9.47 \times 10^{-20}$) $cm^3 molecule^{-1} s^{-1}$ [20]. For this reaction particularly, the reduction of the exit hole to increase the reaction time was dangerous due to the explosive characteristics of the reactant mixture at high pressure. An alternative way to extend the reaction time is to increase the mixing distance using an open ended tube (which was increased to ≈ 10 meter length). In order to build a system which is easy to work with, and taking into account the dimensions of the laboratory, plastic tube was chosen as the material for the inlet tube. The tube was wound as a helix with several mixing points as shown in Figure 2.7. One of the reactants was allowed into the system at the far end of the tube and the other could be added through one of the several mixing points. In this way, several different mixing distances are obtained. This system allows the possibility of changing the total mixing distance by changing the distance between the mixing points over the range of 0 – 10 meters. Because large mixing distances are used, it is not suitable for detection of short lived intermediates (e.g. OH) but it is useful for studying long-lived intermediates or products of slow reactions.

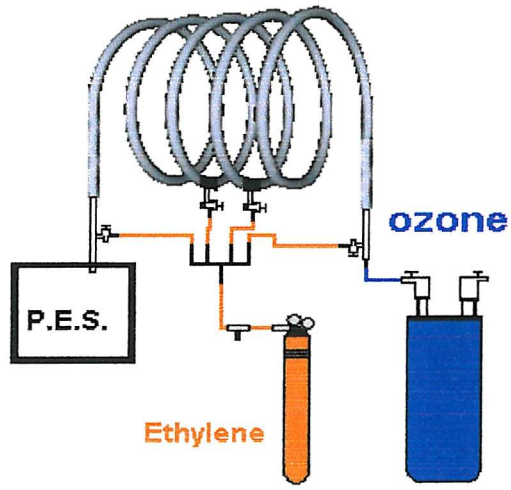

Figure 2.7: Schematic diagram of the Long Inlet System.

The photoelectron spectrometer and the different inlet system described in this section have been used to study the reactions of atmospheric importance and the results obtained are described in Chapters 4 and 5.

- **2.2 References**

[1] J.M. Hollas "*Molecular Spectroscopy*" *Wiley. Chichester* (1987).

[2] A. Einstein *Ann. Physik* **31** (1905) 132.

[3] K. Siegbahn and K. Edvarson *Nucl. Phys.* **37** (1956) 137.

[4] M.I. Al-Joboury and D. W. Turner *J. Chem. Phys* **37** (1962) 3007.

[5] F.I. Vilesov, B. L. Kurbativ and A. N. Terenin *Dokl. Akad. Nauk. SSSR* **138** (1961) 1329.

[6] J. W. Rabalais *"Principles of u.v. PES"* *J. Wiley & Sons. New York* 1977.

[7] J. Berkowitz *"Photoabsorption, Photoionization and Photoelectron Spectroscopy"* *Academic Press. New York.* 1979.

[8] D. Bulgin, J. M. Dyke, F. Goodfellow, N. Jonathan, E. Lee and A. Morris *J. Elec. Spec. Rel. Phem.* **12** (1977) 67.

[9] J. M. Dyke, B. W. J. Gravenor, G. D. Josland, R. A. Lewis and A. Morris *Mol. Phys.* **53** (1984) 465.

[10] J. A. R. Samson
"Techniques of Vacuum Ultraviolet Spectroscopy"
Wiley Interscience, New York (1967)

[11] J. W. Rabalais
"Principles of Ultraviolet Photoelectron Spectroscopy"
Wiley Interscience, New York (1997)

[12] J. A. R. Samson
Rev. Sci. Instrum. **40** (1969) 1174

[13] J. H. D. Eland
"Photoelectron Spectroscopy"
Butterworths, London (1984)

[14] A. Morris, J. M. Dyke, G. D. Josland, M. P. Hastings and P. D. Francis
High Temp. Sci. 22 (1986) 95

[15] A. M. Ellis, *PhD Thesis*, University of Southampton (1989)

[16] A. Morris. *"The Measurements of Ionization Potentials"*
Lecture Notes, University of Southampton.

[17] A. Pouline and D. Roy
J. Phys. E: Sci. Instrum. **11** (1978) 35

[18] I. R. Trickle, *PhD Thesis*, University of Southampton (1980)

[19] M. J. Winter, *PhD Thesis*, University of Southampton (1981).

[20] Japar, S.M.; Wu, C.H.; Niki, H.
J. Phys. Chem. **80** (1976) 2057

CHAPTER 3.

Principles of Photoelectron Spectroscopy

• 3.0 Theoretical Methods [1-5].

A number of important pieces of information may be obtained from experimental molecular photoelectron spectra. These are the adiabatic and vertical ionization energies of a band, vibrational separations associated with any observed vibrational structure and relative intensities of vibrational components in a band. In this chapter, theoretical methods which may be used to calculate these quantities are described. This allows comparison between experimental values and calculated quantities, and therefore provides a valuable tool in the assignment of bands.

In this chapter a brief introduction of molecular orbital theory will be presented and the Hartree-Fock method will be outlined. Koopmans' theorem will also be described and its limitations discussed.

• 3.1 Selection Rules in PES [6-7].

Molecular photoionization is a scattering process, not a resonance process, with ionization being induced by the interaction of the molecule with the electric field of the radiation. The main electronic selection rule for this process is simple: only one-electron ionizations are allowed [6,7]. A spin selection rule also exists which states that photoionization is allowed between initial and final states of the same total spin, i.e. $\Delta S=0$, where the final state consists of the ion plus the free electron. Most stable molecules have closed-shell singlet ground states and their photoelectron spectra show bands which correspond to ionizations from the closed-shell ground state to doublet states of the cation obtained by removal of one electron.

Vibrational structure, described in section 3.2, is often observed in molecular photoelectron bands, particularly of light molecules, and there are vibrational selection rules which control which vibrations may be excited on ionization [7]. Vibrational structure in a photoelectron band is considered in the next section.

- **3.2 Vibrational Structure Observed in Photoelectron Bands [6, 7].**

The resolution of a u.v. photoelectron spectrometer is typically 200 cm^{-1}. This allows resolution of vibrational structure but not rotational structure in a photoelectron band of a molecule. Three principal quantities may be obtained from a vibrationally resolved band, the adiabatic and vertical ionization energies and the vibrational interval(s). The adiabatic ionization energy (AIE) is defined as the difference in energy between the molecule in its ground electronic and vibrational state, and the ion in its lowest vibrational level for a given electronic state. In a photoelectron spectrum the AIE is usually the first component observed in a vibrationally resolved band. The vertical ionization energy (VIE) is defined as the vibrational component in a band corresponding to the transition between the molecule in its ground electronic and vibrational state to the vibrational level in the ion with the greatest overlap with the ground state vibrational wavefunction (i.e. the largest Franck-Condon factor).

A potential energy curve can be used to represent the total energy of a diatomic molecule as a function of the internuclear distance. On such a curve, the total energy is at a minimum when the internuclear distance is equal to R_e, the equilibrium bond length for the molecule. Vibrational energy in a molecule is quantized; the allowed vibrational energies are the solution of the vibrational Schrödinger equation with a chosen form of the potential. If a small displacement, R, from the equilibrium separation, R_e, is considered, the potential energy curve may be approximated to a parabola and expressed as:

$$V(R) = \tfrac{1}{2}\, k_e(R-R_e)^2 \qquad (3.0)$$

This is the potential energy expression for a simple harmonic oscillator. In this equation, V(R) is the potential energy and k_e is the force constant of the bond. Solution of the vibrational Schrödinger equation with this potential energy expression leads to eigenvalues which can be written as:

$$E_{vib} = (v + \tfrac{1}{2})\, \omega_e \qquad (3.1)$$

In equation (3.1), v, is the vibrational quantum number and ω_e is the vibrational constant for the bond. ω_e can be expressed in terms of the force constant, k_e, as:

$$\omega_e = (1 / 2\pi c) \times (k_e / \mu)^{1/2} \qquad (3.2)$$

In equation (3.2), c is the velocity of light and μ is the reduced mass of the molecule. Equation (3.1) breaks down at high vibrational energies as the potential energy curve for a simple harmonic oscillator is not applicable to a potential energy curve for a molecular state. This is because for high vibrational quantum numbers, the repulsive force between the nuclei at small R is high and at large R, the molecule dissociates. As result, the potential energy curve is anharmonic.

An improved expression for the potential energy is the Morse potential [8] which may be written as:

$$V(R) = D_e \{ 1 - \exp (-\alpha (R - R_e) \}^2 \qquad (3.3)$$

where D_e is the dissociation energy and α is a constant. Solution of the vibrational Schrödinger equation with the Morse potential [6] results in eigenvalues given by:

$$E_{vib} = (v + \tfrac{1}{2}) \omega_e - (v + \tfrac{1}{2})^2 \omega_e x_e \qquad (3.4)$$

In equation (3.4), x_e is an anharmonicity constant, v is the vibrational quantum number and ω_e is the vibrational constant. From equation (3.4), it may be shown that the separation between successive vibrational levels in a state is not constant, as in the case for a simple harmonic oscillator, but the vibrational levels get closer together. This separation of adjacent levels may be written as:

$$\Delta E = E (v + 1) - E (v) = \omega_e - 2 \omega_e x_e (v + 1) \qquad (3.5)$$

For a chosen molecule, if the separation of the first and second vibrational levels in the ground electronic state is very much larger than k_BT at room temperature, then all the molecules will be in the lowest vibrational level (v''=0). Vibrational structure observed within a photoelectron band will then be the result of ionization to successive vibrational levels in the ion. If the observed vibrational separations, ΔE, are plotted against (v+1), a straight line is obtained with slope $-2\omega_e x_e$ and intercept ω_e. Thus the vibrational parameters, ω_e and $\omega_e x_e$ for a given ionic state may be obtained in this way, provided the vibrational numbering is established. Furthermore, comparison of the derived value of ω_e in the ionic state with the neutral molecular ω_e value may be provide insight into the nature of the bonding character of the molecular orbital from which ionization has occurred.

Ionization from a non-bonding orbital results in little change in the internuclear bond length and vibrational constant (ω_e) on ionization. As a result the corresponding photoelectron band will show similar vibrational separations to those in the neutral molecule. An intense adiabatic component with a short progression of weaker bands to higher ionization energy is observed, as in the case of the first bands of water [9] and the methyl radical [10]. A broad vibrational progression in which the adiabatic and vertical components are not equal is indicative of ionization from a bonding or non-bonding orbital. Comparison of the vibrational intervals with those in the neutral shows a decrease in vibrational separation associated with a weakening of the bond in the case of ionization from a bonding orbital. A corresponding increase in vibrational separation, indicating a strengthened bond is observed on ionization from an antibonding orbital.

Photoionization from a ground molecular state to the ground and first excited ionic states of a molecule and the expected photoelectron band envelopes are shown schematically in Figure 3.1.

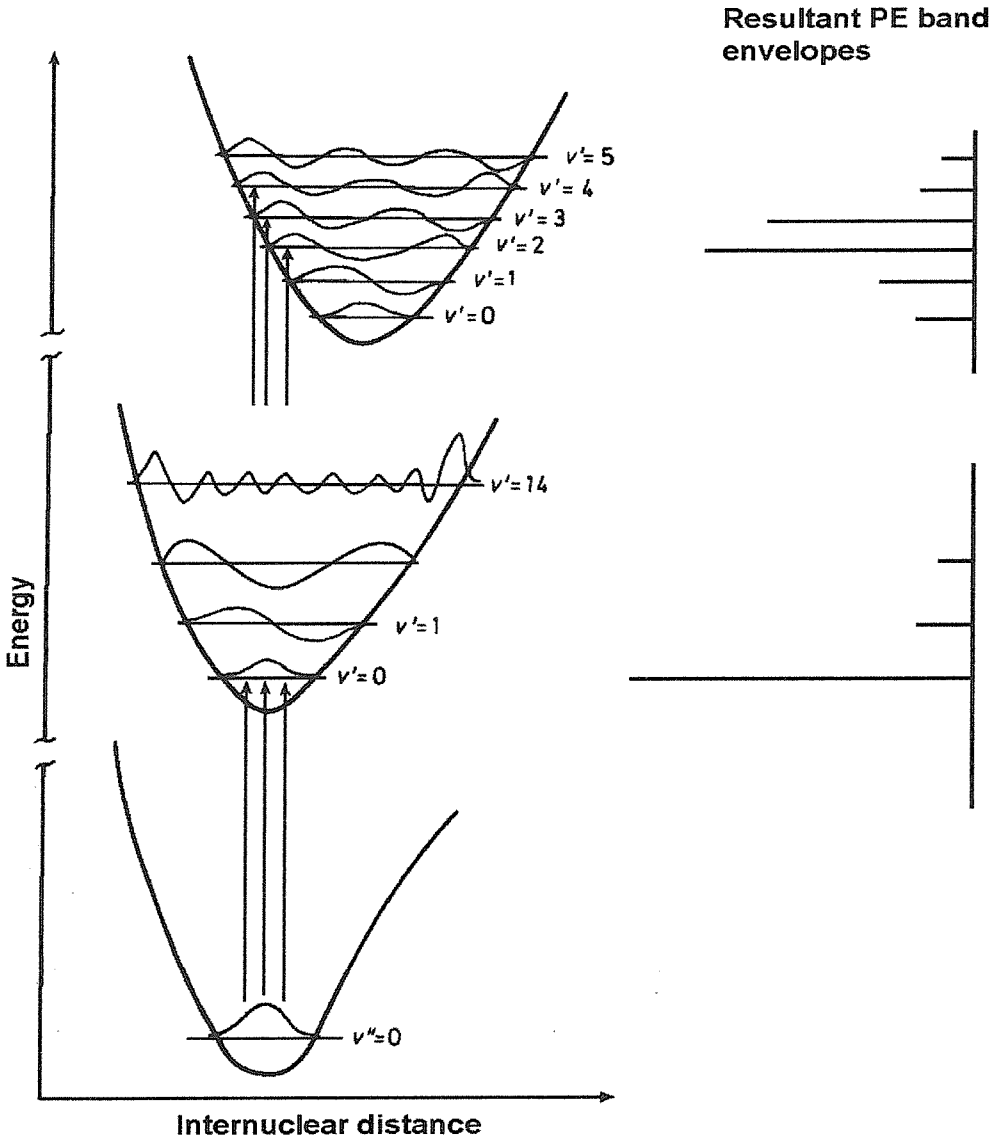

Figure 3.1: Schematic diagram of ionization from the ground molecular state to the ground ionic state, and ionization from the ground molecular state to the first exited state of the ion with the expected photoelectron band envelopes.

- **3.3 Relative Intensity within a Vibrationally resolved Photoelectron Band [6, 7].**

The photoelectron process is very rapid. An electron is ejected from an atom or molecule within 10^{-15}s after the interaction with the ionizing photon [6]. In a classical picture, molecular vibrations occur on a timescale of 10^{-13}s hence the molecular coordinates are effectively frozen on the photoionization timescale for the most probable vibrational transition in a band.

For a diatomic molecule, the Frank-Condon principle [6] states, that the intensity of a vibrational component in an electronically allowed band is proportional to the square of the modulus of the overlap of the initial and final vibrational wavefunctions, $\Psi_{v''}$ and $\Psi_{v'}$. This may be expressed as:

$$I_{v' \leftarrow v''} \alpha | \int \Psi_{v'}(R) \Psi_{v''} dR|^2 \qquad (3.6)$$

In equation (3.6) it is assumed that the electronic transition moment is constant across the photoelectron band. This assumption is good for short vibrational progressions but an error may be introduced for broad progressions.

- **3.4 The calculation of Molecular Ionization Energies [14, 15].**

In order to assist in the assignment of molecular photoelectron spectra, calculation may be made of molecular ionization energies and neutral and ionic vibrational constants. The calculations involve molecular orbital calculations which provide approximate solutions of the time-independent electronic Schrödinger equation:

$$H \Psi = E \Psi \qquad (3.7)$$

In equation (3.7), H is the electronic Hamiltonian, E is the total energy of a molecular state and Ψ is the wavefunction of the state. It is only possible to solve this equation exactly for hydrogen-like atoms and the molecular hydrogen cation,

H_2^+ [11]. In order to obtain solutions to the Schrödinger equation for larger systems with more electrons, it is necessary to introduce a number of approximations.

The first approximation that is made is the Born-Oppenheimer approximation [12]. This states that the nuclear and electronic motions of a molecule can be separated. Molecular orbital theory is concerned with calculating total electronic energies and wavefunctions within the Born-Oppenheimer approximation. As the electrons move much faster than the nuclei, within the Born-Oppenheimer approximation, on an electronic timescale the nuclei can be considered as fixed. The total energy of the system may then be expressed as the sum of the electronic and nuclear terms:

$$E_{tot} = E_{elec} + E_{nucl} \tag{3.8}$$

For a fixed nuclear configuration of a system, comprising n-electrons, the electronic Hamiltonian may be written:

$$H_{elec} = \underset{(1)}{-\tfrac{1}{2}\sum_\zeta \nabla^2\zeta} \quad \underset{(2)}{-\sum_\alpha\sum_\zeta z_\alpha / r_{\zeta\alpha}} \quad \underset{(3)}{+\sum_\eta\sum_\zeta 1/r_{\eta\zeta}} \tag{3.9}$$

In this equation, α refers to the nuclei and ζ and η refer to the electrons. In this equation, the first term (1), represents the kinetic energy of all the electrons in the system. Term (2) represents the attractive potential between the electrons and the nuclei, where $r_{\zeta\alpha}$ is the distance between nucleus α and electrons ζ. z_α represents the charge on nucleus α. The third term represents electron-electron interaction between electrons ζ and η. For many electron systems, it is this electron-electron interaction term which gives computational difficulties and makes the electronic Schrödinger equation insoluble analytically. As a result, in addition to the Born-Oppenheimer approximation mentioned previously, the orbital approximation is also required in order to obtain approximate solutions for the Schrödinger equation. The orbital approximation considers the motion of each electron in the system as separate one-electron functions, or spin orbitals, λ_i. The total electronic wavefunction is then formulated as a product of one-electron

functions which must satisfy the Pauli exclusion principle. The Pauli Exclusion Principle [13] states that the total electronic wavefunction must be antisymmetric with respect to interchange of two electrons (which are fermions).

A function which satisfies this invariance condition is the Slater determinant [14] which is written as:

$$\Psi = 1/\sqrt{n!} \times \begin{vmatrix} \lambda_1(1) & \lambda_2(1) & \lambda_3(1) \\ \lambda_1(2) & \lambda_2(2) & \lambda_3(2) \\ \lambda_1(3) & \lambda_2(3) & \lambda_3(3) \end{vmatrix} \qquad (3.10)$$

In equation 3.10, n is the number of electrons in the system and the spin-orbitals are written as $\lambda_i(\zeta)$. The spin-orbitals are assumed to be orthonormal such that:

$$\int \lambda_i \lambda_j \, d\tau = \delta_{ij} \qquad (3.11)$$

where δ_{ij} is the Kronecker delta which is equal to 1 if i=j and 0 if i≠j. The Slater determinant [14] is therefore an approximation to the true electronic wavefunction. It is based on the orbital approximation. Also, space and spin parts of $\lambda_i(\zeta)$ can be separated if relativistic effects in the molecular system considered are small. For a given approximate wavefunction, expressed in terms of some disposable parameters, the Variation Method allows the lowest total energy to be obtained subject to minimization of the total energy with respect to these parameters.

- *3.4.1 The Variational Method [15].*

A true wavefunction, Ψ, of a system satisfies the Schrödinger equation (3.7). The true energy, E, may be calculated if Ψ is known. This is achieved by multiplying both sides of equation (3.7) by Ψ^* and integrated over all space to give:

$$E_{true} = \frac{\int \Psi^* H \Psi \, d\tau}{\int \Psi^* \Psi \, d\tau} \qquad (3.12)$$

If Ψ is not an exact wavefunction, but a trial wavefunction, Ψ_t may be expressed in terms of the true eigenfunctions of the system as follows:

$$\Psi_t = \Sigma_i \, c_i \, \Psi_i \qquad (3.13)$$

The expression for the energy E_{trial} calculated from a trial wavefunction is therefore:

$$E_{trial} = \frac{\int \Psi^* H \Psi \, d\tau}{\int \Psi^* \Psi \, d\tau} \qquad (3.14)$$

It may be shown that the difference in energy between the true and trial wavefunctions is always greater than, or equal to zero [14]. The Variation Theorem states that the energy calculated from a trial wavefunction is always greater than or equal to the true energy of the system. Hence the "best" representation of the wavefunction is the one which gives the lowest total energy.

- *3.4.2 The Hartree-Fock Method [1-3].*

This chapter does not intend to present a detailed derivation of the Hartree-Fock method as it is contained in many good texts. Rather a broad overview of the underlying concepts and the validity of the equations and computed quantities obtained from this theory will be considered.

A variational method for solving the Schrödinger equation numerically for a closed-shell system was first put forward by Hartree [1] and was known as the self-consistent field method. This approach was modified to include electron exchange effects by Fock and gave rise to the Hartree-Fock SCF theory [2, 3].

Hartree-Fock (HF) theory includes electron-electron interactions unlike more primitive methods such as Hückel theory [15]. In Hartree-Fock theory,

electron-electron interaction is represented by coulomb and exchange terms and in this method the coulomb term is evaluated as the interaction of each electron with an average charge of all the others. The exchange term is defined as the interaction of an electron with other electrons of the same spin.

The basic aim of the Hartree-Fock (HF) Self Consistent Field (SCF) method is to obtain the best single determinantal wavefunction for a closed shell system containing N electrons, of the general form:

$$\Delta_N = (\Phi_1\bar{\Phi}_1\Phi_2\bar{\Phi}_2 \ldots \Phi_v\bar{\Phi}_v) \qquad (3.15)$$

where v = N/2 and a bar superscript denotes β spin, no bar denotes α spin. Equation (3.15) is an antisymmetrised determinant (equation 3.10) written in terms of space orbitals (Φ_i). For such a closed-shell system, the following expression for the total energy may be derived [1-3]:

$$E_{TOT} = 2\,\Sigma_i\, I_i + \Sigma_{ij}\,(2J_{ij} - K_{ij}) \qquad (3.16)$$

In this equation i and j range from 1 to N/2 space orbitals. The term I_i is the energy possessed by an electron in orbital i, moving in the field of the nuclei. The coulomb integral, J_{ij}, represents the coulombic interaction between electrons in space orbitals i and j. The exchange integral, K_{ij}, has no classical analogue and arises as a result of the antisymmetrising condition which is imposed on the trial wavefunction.

The coulomb integral J_{ij} may be written as:

$$J_{ij} = \int\int \phi_i^*(1)\,\phi_j^*(2)\;\; 1/r_{ij}\;\; \phi_i(1)\,\phi_j(2)\;\; d\tau \qquad (3.17)$$

Also, the exchange integral K_{ij} may be written as:

$$K_{ij} = \int\int \phi_i^*(1)\,\phi_j^*(2)\;\; 1/r_{ij}\;\; \phi_j(1)\,\phi_i(2)\;\; d\tau \qquad (3.18)$$

Using these equations and the linear combination of atomic orbitals (LCAO) expression:

$$\Phi_i = \Sigma_q \, c_{iq} \chi_q \tag{3.19}$$

and applying the Variational Theorem to equation (3.16), the Roothaan-Hall secular equations may be derived [16]:

$$\Sigma_p \, c_{ip} (F_{pq} - \varepsilon_i S_{pq}) = 0 \tag{3.20}$$

In this equation, S_{pq} is the overlap integral between basis functions X_p and X_q. F_{pq} is a matrix element of H with functions X_p and X_q. I_{pq} is the one-electron integral, defined in terms of space orbitals as:

$$I_{ij} = \int \phi_i^*(1) \, H_{N(1)} \, \phi_j(1) \, d\tau(1) \tag{3.21}$$

where $H_{n(1)}$ represents the full molecular Hamiltonian without electron-electron interaction terms. Two-electron integrals with respect to atomic orbitals are represented by:

$$\langle pq \mid rs \rangle = \int\int X_p(1) X_r(2) \, 1/r_{k12} \, X_q(1) X_s(2) \, dv(1) dv(2) \tag{3.22}$$

where the indexes p, q, r and s in equation (3.22) are reserved for atomic orbitals. Unfortunately equation (3.20) cannot be solved because the F_{pq} matrix element depends on the coefficients (c_{iq}) through the expression:

$$F_{pq} = I_{pq} + \Sigma_j \, [\, 2 \, (pq/jj) - (pj/qj) \,] \tag{3.23}$$

As $\Phi_j = \Sigma_q \, c_{jq} \chi_q$, F_{pq} can be rewritten as:

$$F_{pq} = I_{pq} + \Sigma_j \Sigma_r \Sigma_s \, c_{jr} \, c_{js} \, [2 \langle pq \mid rs \rangle - \langle pr \mid qs \rangle] \tag{3.24}$$

Hence F_{pq} is not known until c_{ij} and c_{jq} are known and F_{pq} is needed to obtain these coefficients. To solve this problem, an iterative method is applied where initially some coefficients (c's) are chosen to obtain a trial F_{pq}. The procedure used may be summarized as follows:

1. A selected basis set of atomic orbital functions (X_p) is chosen. In general, the larger the basis set, the more accurately the molecular orbitals are represented, resulting in a lower computed total energy.
2. The overlap integrals S_{pq}, the one electron integral I_{pq} and the two electron integrals (pq | rs) are evaluated.
3. An estimate is made for the values of the coefficients (C_{jq}).
4. The electron-electron interaction integrals (pq | jj) and (pj | jq) are then evaluated.
5. Using the values of the integrals calculated in step (2) and (4), F_{pq} terms are evaluated and the molecular orbital energies are calculated. This may be achieved by solving the determinant $|F_{pq}-\varepsilon S_{pq}|=0$.
6. For each computed orbital energy, ε, equation (3.20) can be solved to obtain the coefficients.
7. The total energy is then computed. The new coefficients are then used in step (3) and the process repeated. If the total energy computed on the next cycle differs from the previous total energy by more than a pre-set tolerance the process is continued. In practice, usually on successive cycles the total energy becomes more negative. If the energy difference is less than a pre-set tolerance then the cyclic process is terminated and the solution accepted.

This solution is known as the Self-Consistent-Field Solution (SCF). The energy obtained in this way is called the Hartree-Fock-SCF total energy. If the total SCF energy cannot be made more negative by increasing the size of the basis set, the Hartree-Fock limit is said to have been reached. The total energy obtained in this way is always higher than the true energy of the system, principally due to a problem of electron correlation which will now be examined.

- *3.4.3 Electron Correlation [4-16].*

The difference between the total energy calculated at the Hartree-Fock limit and the exact non-relativistic total energy of a system is defined as the correlation energy. The correlation problem arises from having used a product of one electron orbitals in a single determinantal function and hence electronic motion is not properly correlated. The neglect of electron correlation in the Hartree-Fock method results in total energies which are higher than the "true" energy and potential energy curves which are steeper than the true curves. The incorrect form of the potential energy curve obtained from Hartree-Fock level calculations results in values for D_e, the dissociation energy which are greater than experimental values, low values for r_e, the equilibrium internuclear separation, and values of ω_e which are greater than the experimental values. For a given state, the true non-relativistic total energy (E_{exact}) can be written as:

$$E_{exact} = E_{Hartree\text{-}Fock} + E_{correlation} \qquad (3.25)$$

The magnitude of the error caused by the neglect of electron correlation usually increases with the number of electrons present in the system, and hence this error will be larger for a neutral species than for a cation. This results in calculated ionization energies obtained from Hartree-Fock SCF total energies of a molecule and a cation which are higher than the experimental values.

Two types of electron correlation can be defined, dynamical and non-dynamical correlation. Dynamical correlation is dependent upon the motion of the electron and is a short-range effect. Non-dynamical correlation is a result of a poor description of an electronic configuration being given by a single Slater determinant and changes with internuclear distance.

- *3.4.4 Koopmans' Theorem [17].*

The simplest method to compute vertical ionization energies is Koopmans' theorem. This is applicable only to closed-shell molecules where ionization from each occupied orbital results in only one band in the photoelectron spectrum. Koopmans' theorem states that the i th vertical ionization energy is equal to the negative of the i th molecular orbital energy, obtained from a SCF calculation carried out at the Hartree-Fock limit on the ground state of the neutral molecule. i.e.

$$I_q^0 = -\varepsilon_q \qquad (3.26)$$

where I_q^0 is the Koopmans' theorem vertical ionization and ε_q is an occupied orbital energy obtained from an SCF calculation at the Hartree-Fock limit.

The major assumption of Koopmans' theorem is that the molecular orbitals (i.e. the c_{iq}'s for each ε) are unchanged on going from the molecule to the ion. In practice there is a change in the molecular orbital coefficients and energies upon ionization. This is due to orbital relaxation; the molecular orbitals in the ion change upon removing an electron and this results in the change in the coefficients in each linear combination of atomic orbitals for each orbital and a change in orbital energies. Neglect of orbital relaxation results in computed vertical ionization energies which are generally higher than the experimental values. By carrying out separate SCF calculations on the neutral and ionic state and subtracting the two SCF total energies (the ΔSCF method), allowance for orbital relaxation can be made. However, the effect of electron correlation will be neglected at the Hartree-Fock SCF level for both the molecule and the ion, and this limits the accuracy of such calculation. Koopmans' theorem VIEs may be related to experimental VIEs by:

$$I_q = I_q^0 - R + C \qquad (3.27)$$

In equation (3.27), I_q is the experimental vertical ionization energy, I_q^0 is the Koopmans' theorem value, R is the electron reorganization term and C is the electron correlation correction which is equal to the difference in the correlation energy in the molecular and ionic state. In practice, the R and C terms tend to cancel each other resulting in reasonably accurate calculation of vertical ionization energies. However, this result is not guaranteed and Koopamns' theorem must in general be applied with caution. In general, Koopmans' theorem vertical ionization energies will be too high when compared to experiment. In order to calculate ionization energies beyond the Koopmans' limit, methods must be used which take into account electron correlation in each state and represent more accurately the form of the molecular orbitals in the molecule and the ion.

- *3.4.5 Møller-Plesset Perturbation Theory [20].*

Møller-Plesset Perturbation theory (MP) is a way of estimating the electron correlation energy associated with an SCF wavefunction using perturbation theory. The method treats the complete Hamiltonian as the sum of two parts, the first part being the Hartree-Fock one-electron solution and the second a perturbation Hamiltonian. This may be represented as:

$$H_\lambda = H_0 + \lambda V \qquad (3.29)$$

In this equation, H_λ is the correct Hamiltonian, and λ is a dimensionless parameter. H_0, the zero order Hamiltionan, is taken to be the sum of the one-electron Fock operators. The perturbation, λV is defined:

$$\lambda V = (H_\lambda - H_0) \qquad (3.30)$$

The method follows standard Rayleigh-Schrödinger perturbation theory [20] in that the exact ground state wavefunction, φ_λ, within a given basis set is expressed as:

$$\varphi_\lambda = \varphi^{(0)} + \lambda\varphi^{(1)} + \lambda\varphi^{(2)} \quad (3.31)$$

and the exact ground state energy, E_λ, is expressed as:

$$E_\lambda = E^{(0)} + \lambda E^{(1)} + \lambda^2 E^{(2)} + \ldots \quad (3.32)$$

A practical correlation method may be formulated if λ is set equal to 1 and the series truncated to various orders. The name of the method is given by the highest order energy term. For example truncation after the fourth order term is known MP4. MP theory is size consistent, which means that applying the model to a system of molecules at infinite separations results in properties that are equal to the sum of the same properties for the individual molecules.

However all perturbation theory methods regardless of order of termination are not variational due to the method of derivation.

- *3.4.6 Basis Sets [21].*

The choice of basis set (i.e. the X_p's) used in an *ab initio* molecular calculation is largely determined by the nature of the molecule and molecular state being investigated and the computing power and storage available. The most computationally time consuming step of an SCF calculation is the evaluation of the two-electron integrals (described in section 3.4.2). The number of such integrals is proportional to the fourth power of the number of basis functions. In practice a trade off between computational expense and the quality of the calculation is made.

In practice, two types of basis functions are used in modern molecular orbital calculation to describe atomic orbitals, Slater-type orbitals (STOs) [22] and Gaussian-type (GTOs) [23]. Most modern methods employ GTOs as they lead to two-electron integrals which may be evaluated analytically unlike STOs, which lead to two-electron integrals which must be evaluated numerically. However, STOs are a better representation of "real" atomic orbitals. Hence, more GTOs need to be

used than STOs to obtain the same accuracy. A number of different types of basis set will now be described.

The minimum Basis set.

At the simplest level of *ab initio* molecular orbital theory, a minimum basis set of nuclear-centered functions may be used. A minimum atomic basis set is one in which one GTO or STO function is used for each formally occupied atomic orbital in an atom. Practical experience shows that is often necessary to include extra functions. Minimal basis sets have several deficiencies. The main problem is a lack of flexibility to represent responses to a change in molecular environment. These deficiencies may be overcome by using more than one function for each formally occupied orbital in an atom. For example, by employing two s-type basis functions, one contracted and one diffuse, a function is obtained which may vary radically between the contracted and diffuse limits.

Polarisation Basis Sets [21].

Most commonly used basis functions are constrained to be centred at nuclear positions. For highly polar molecules (e.g. HF) and molecules comprising small, strained rings, allowance must be made for displacement of the charge away from atomic centers. One way to allow for this displacement is to incorporate functions of high angular quantum number (e.g. p-type functions for hydrogen and d-type functions for first row elements) in the basis set which are formally unoccupied in an atom. The incorporation of functions of higher angular quantum number than are required for the atom in its electronic ground state results in a polarization basis set.

*The 6-311G** Polarisation Basis set [21].*

This basis set is used in Gaussian 1 and 2 calculations [4, 5]. In this basis set, the valence region is split into three, one, and one Gaussian functions, and the inner shell is represented by six s-type Gaussian functions. Splitting in this way increases the flexibility of the representation and gives a better description of the valence region than the non-split basis set. The basis is supplemented for first-row atoms by a set of five d-type Gaussian polarization functions and one p-type polarization Gaussian function for hydrogen. The two stars indicate that this basis set incorporates these polarization functions.

In this work the minimum energy geometries and vibrational frequencies of the complex CH_3SCH_2Cl:HCl and DMS:Cl_2 were calculated using MP theory truncated at second order (MP2), by Dc. E. Lee of the Southampton PES group, in order to assist the assignment of photoelectron bands associated with intermediate in the reaction DMS+Cl_2. These results are presented in Chapters 4 and 5.

- **3.5 References**

[1] D. R. Hartree
Proc. Camb. Phil. Soc. **24** (1928) 89.

[2] V. Fock
Z. Physik 61 (1930) 161.

[3] D. R. Hartree, W. Hartree and B. Swirles
Phil. Trans. Roy. Soc A. **38** (1939) 229.

[4] J. A. Pople, M. H. Gordon, D. J. Fox, K. Raghavachari and L. A. Curtiss
J. Chem. Phys. **90** (1989) 5622.

[5] L. A. Curtiss, K. Raghavachari, G. W. Trucks and J. A. Pople
J. Chem. Phys. **94** (1991) 7221.

[6] J. H. D. Eland *"Photoelectron Spectroscopy"*
Butterworths, London (1984).

[7] J. W. Rabalais
"Principles of Ultraviolet Photoelectron Spectroscopy"
Wiley, New York (1977).

[8] P. M. Morse
Phys. Rev. **34** (1929) 57.

[9] K. Kimura, S. Katsumata, Y. Achiba, T. Yamazaki and S. Iwata
"Handbook of HeI Photoelectron Spectra of fundamental Organic Molecules"
Japan Scientific Societies Press, Tokyo, 1981.

[10] J. M. Dyke, N. Jonathan, E. Lee and A. Morris
J. Chem Soc. Far. II **72**, (1976) 1385.

[11] P. W. Atkins *"Molecular Quantum Mechanics"*
Second Ed. Oxford University Press, Oxford (1983).

[12] M. Born and R. Oppenheimar
Ann. Phys. **84** (1927) 457.

[13] W. Paulin
Z. Physik **31** (1925) 265.

[14] J. N. Murrell, S. F. A. Kettle and J. M. Tedder
"The Chemical Bond"
J. Wiley & Sons, Chichester. (1990)

[15] R. G. Parr
"The quantum Theory of Molecular Electronic Structure"
W. A. Benjamin, New York. (1964).

[16] C. C. J. Roothaan
Rev. Mod. Phys. **23** (1951) 69.

[17] T. Koopmans
Physica, **1** (1934) 104.

[18] C. C. J. Roothaan
Rev. Mod. Phys. **32** (1960) 179.

[19] J. A. Pople and R. K. Nesbet
J. Chem. Phys. **22** (1954) 571.

[20] C. Møller and M. S. Plesset
Phys. Rev. **49** (1934) 618.

[21] W. J. Hehre, L. Radom, P. V. R. Schleyer and J. A. Pople
"Ab initio Molecular Orbital Theory"
Wiley-Interscience. New York (1986)

[22] J. A. Pople, H. B. Schlegel, R. Krishanan, D. J. Defrees, J. S. Binkley, M. J. Frisch, R. A. Whiteside, R. F. Hout and W. J. Hehre.
Int. J. Quantum. Chem. Symp. **15** (1981) 269.

CHAPTER 4.

Results

- **4.1 Cl_2 + DMS Reaction.**

A photoelectron spectrum recorded for DMS, mixed with Cl_2 at a distance of 15 cm above the photon beam, is shown in Fig. 4.1. The first two bands of DMS can be seen clearly at 8.68 and 11.30 eV vertical ionization energy (VIE)[1] and the first two bands of Cl_2 are seen at 11.59 and 14.40 eV VIE [1]. At higher energies two bands appear (15.76 and 15.94 eV IE) corresponding with the $Ar(3p)^{-1}$ Ar^+ ($^2P_{3/2,1/2}$)← $Ar(^1S_0)$ ionizations that have been used as calibrants in all spectra, together with the first band of DMS or DMDS.

At this reaction distance two bands appear in the region 9.5-10.9 eV. These two bands at 9.65 and 10.55 eV VIE are replaced by bands of CH_3SCH_2Cl and HCl at longer reaction times. They are assigned to the 1:1 complex CH_3SCH_2Cl:HCl as a calculation of the first VIE agrees with the first VIE of the first band associated with the complex as shown in Table 4.1. Initially, it was thought that these bands were associated with the DMS:Cl_2 complex but the first VIE computed by *ab inito* calculations showed poor agreement with the experimental first VIE. The assignment will be discussed in more detail in the next Chapter.

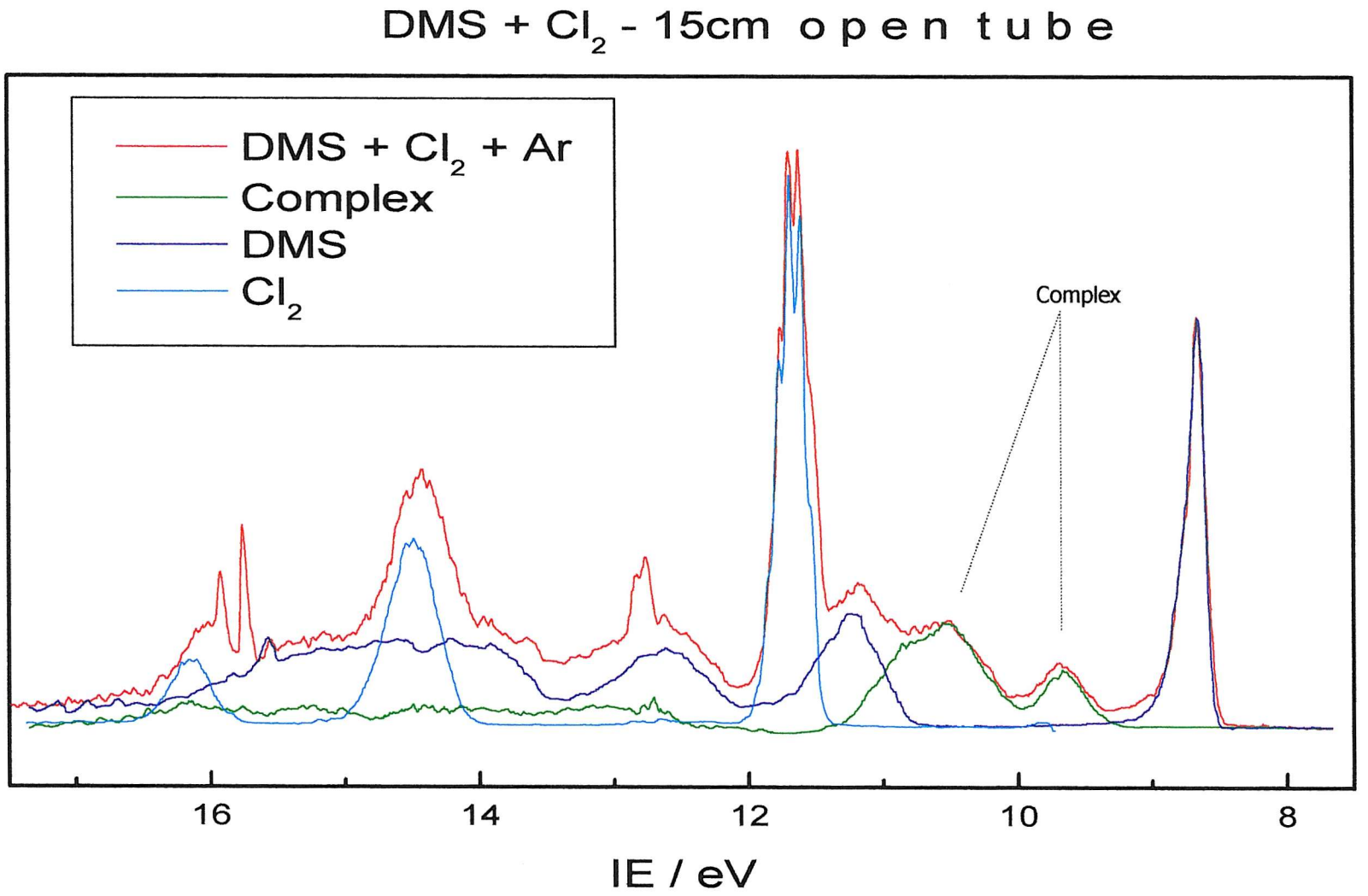

Figure 4.1: Spectra obtained for the Cl_2+DMS reaction recorded with a fixed mixing distance (15 cm) and an open tube. It shows the formation of the complex (bands at 9.6-9.7 and 10.6-10.8 eV). The spectra for the reactants Cl_2 and DMS were obtained at the same partial pressure as in the reaction but separately.

Methods	VIE (eV)	Nbasis
MP2/6-31++G**	9.37	143
MP2(full)/6-31++G**	9.37	143
MP2/aug-cc-pVDZ	9.49	181
MP2/6-31++G(3df,3pd)	9.53	310
MP2/6-311++G(3df,3pd)	9.55	327
RCCSD/aug-cc-pVDZ	9.40	181
RCCSD(T)/aug-cc-pVDZ	9.42	181
RCCSD/aug-cc-pVTZ	9.51	380
RCCSD(T)/aug-cc-pVTZ[a]	9.53	380
Experimental	**9.66**	

Table 4.1: Vertical ionization energy table obtained from *ab-initio* calculations at different levels of calculation for the first vertical ionization of the complex CH_3SCH_2Cl:HCl.

As well as observing bands of the complex,at longer reaction times, new bands appear in the spectrum at 9.16 and 10.86 eV VIE, and bands of HCl at 12.75 and 16.28 eV VIE increase with mixing distance. Figure 4.2 shows how these bands increase with the reaction time. These spectra were recorded with a hole in the outer exit tube of 1 mm, which is smaller than the 12mm exit hole of an open tube.

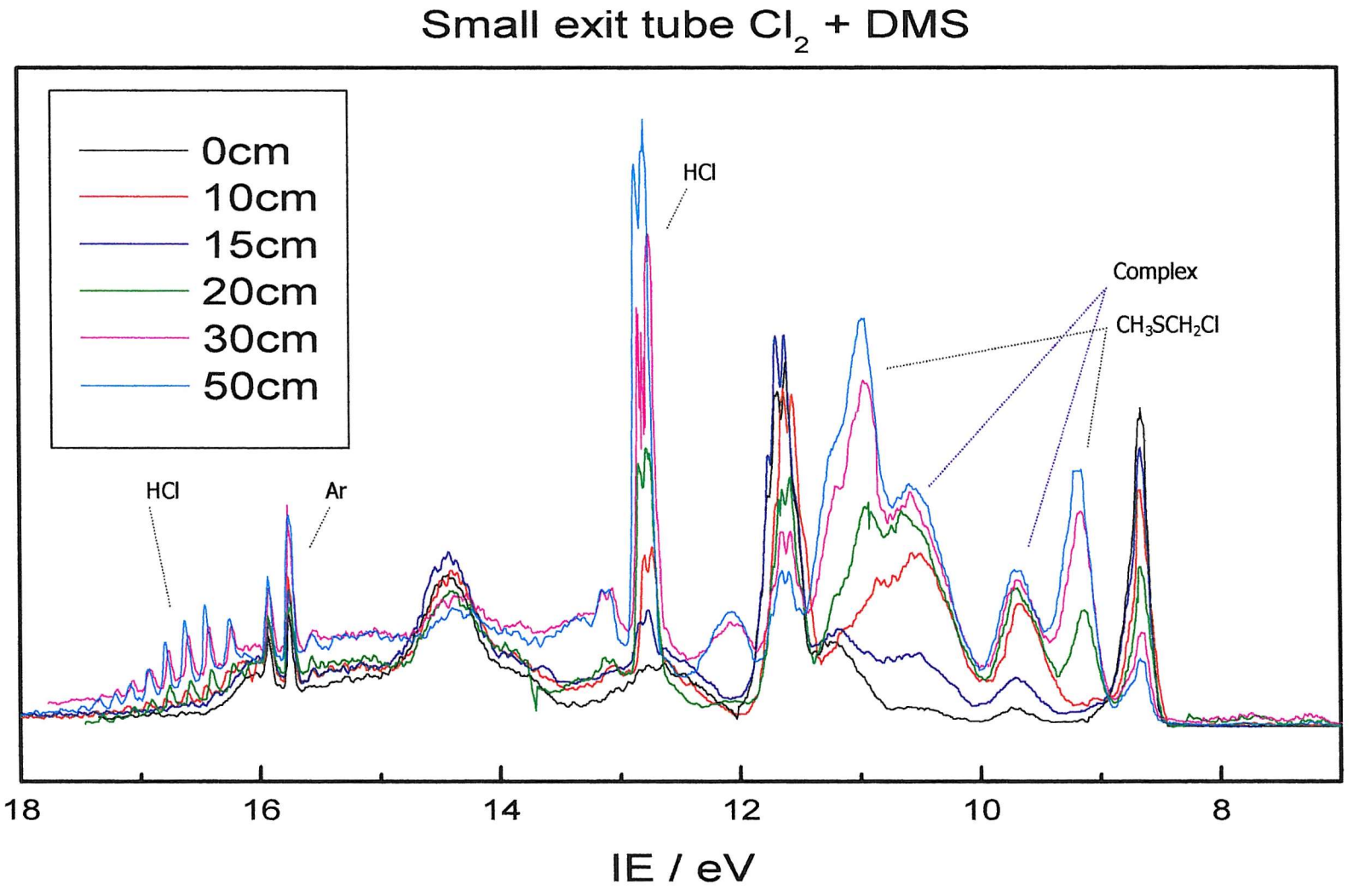

Figure 4.2: Spectra recorded at different mixing distances for the Cl_2+DMS reaction. It can be seen how the formation of CH_3SCH_2Cl (bands at 9.16 and 10.86 eV) and HCl (bands at 12.75 and 16.28 eV VIE) increase with reaction time.

The assignment of the bands shown in Figure 4.2 to CH_3SCH_2Cl is confirmed by recording the He-I photoelectron spectrum of CH_3SCH_2Cl (obtained from Aldrich, 95%) and this is shown in Figure 4.3.

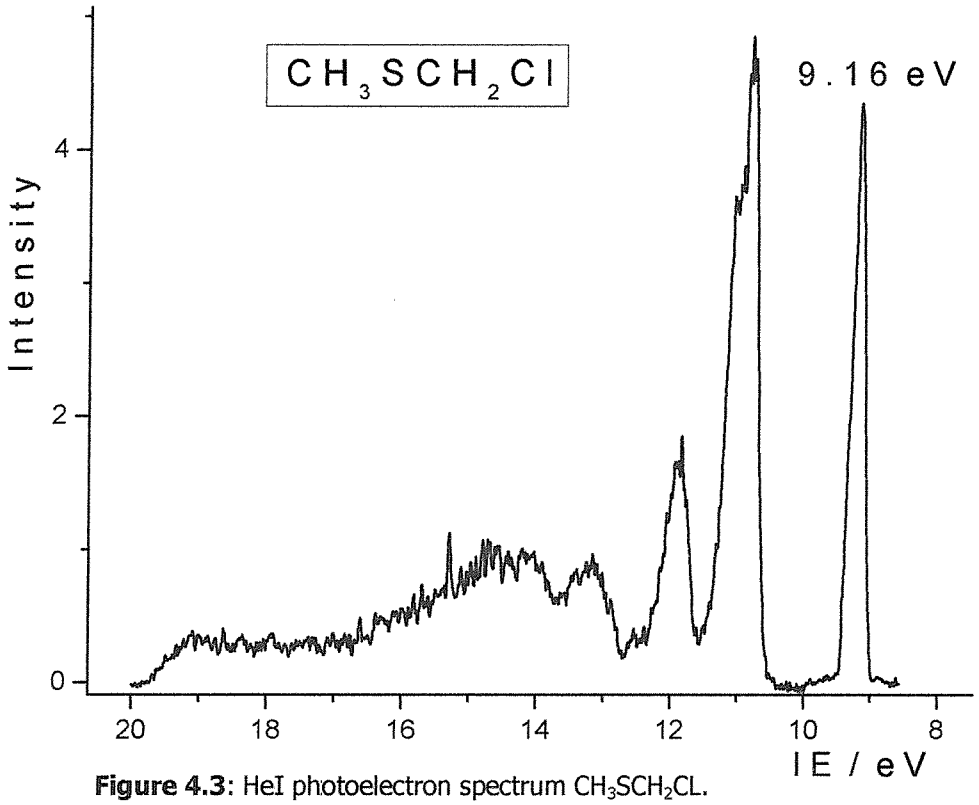

Figure 4.3: HeI photoelectron spectrum CH_3SCH_2CL.

From the relative band intensities measured, for the photoelectron spectra of the reaction DMS+Cl_2, at different mixing distances at constant reagent partial pressure, the band intensity of each species observed can be plotted against mixing distance. This plot is shown in Figure 4.4. From this plot, it can be seen that the complex is formed at intermediate reaction times but it decomposes at later times to give CH_3SCH_2Cl+HCl.

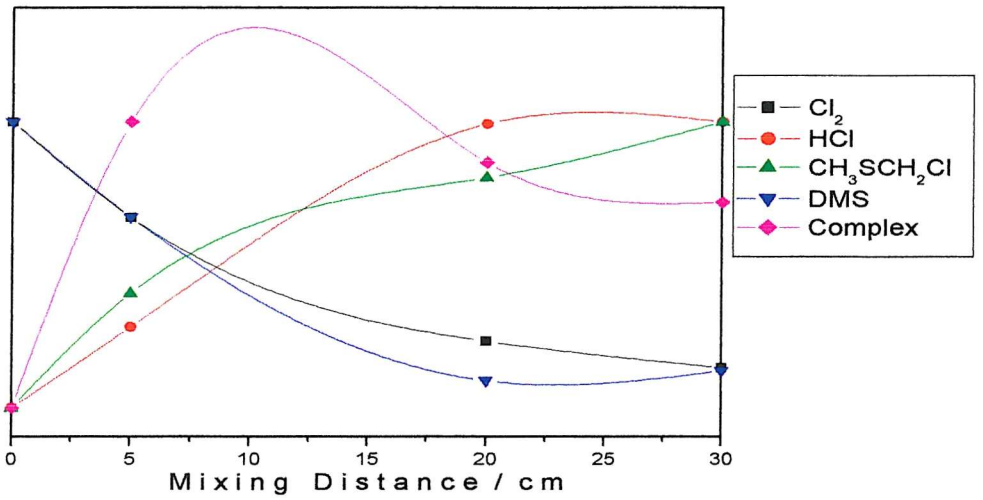

Figure 4.4: Mixing distance plot obtained for the DMS+Cl_2 reaction, with an open inlet tube.

- **4.2 Cl_2 + DMDS Reaction.**

Figure 4.5 shows spectra recorded for the DMDS+Cl_2 reaction using a 1mm exit hole inlet system at different mixing distances. The first two bands of DMDS can be seen at 8.96 and 9.26 eV VIE and the first two bands of Cl_2 are seen at 11.59 and 14.40 eV VIE. As is evident from this diagram, the reaction is not complete even at the longest mixing distance because DMDS is present. At this reaction time new bands appear; the lowest ionization energy feature at 9.21 eV VIE was found to correspond with the product CH_3SCl [5]. Also a weak band at 12.75 eV VIE corresponding to HCl increases with the reaction time.

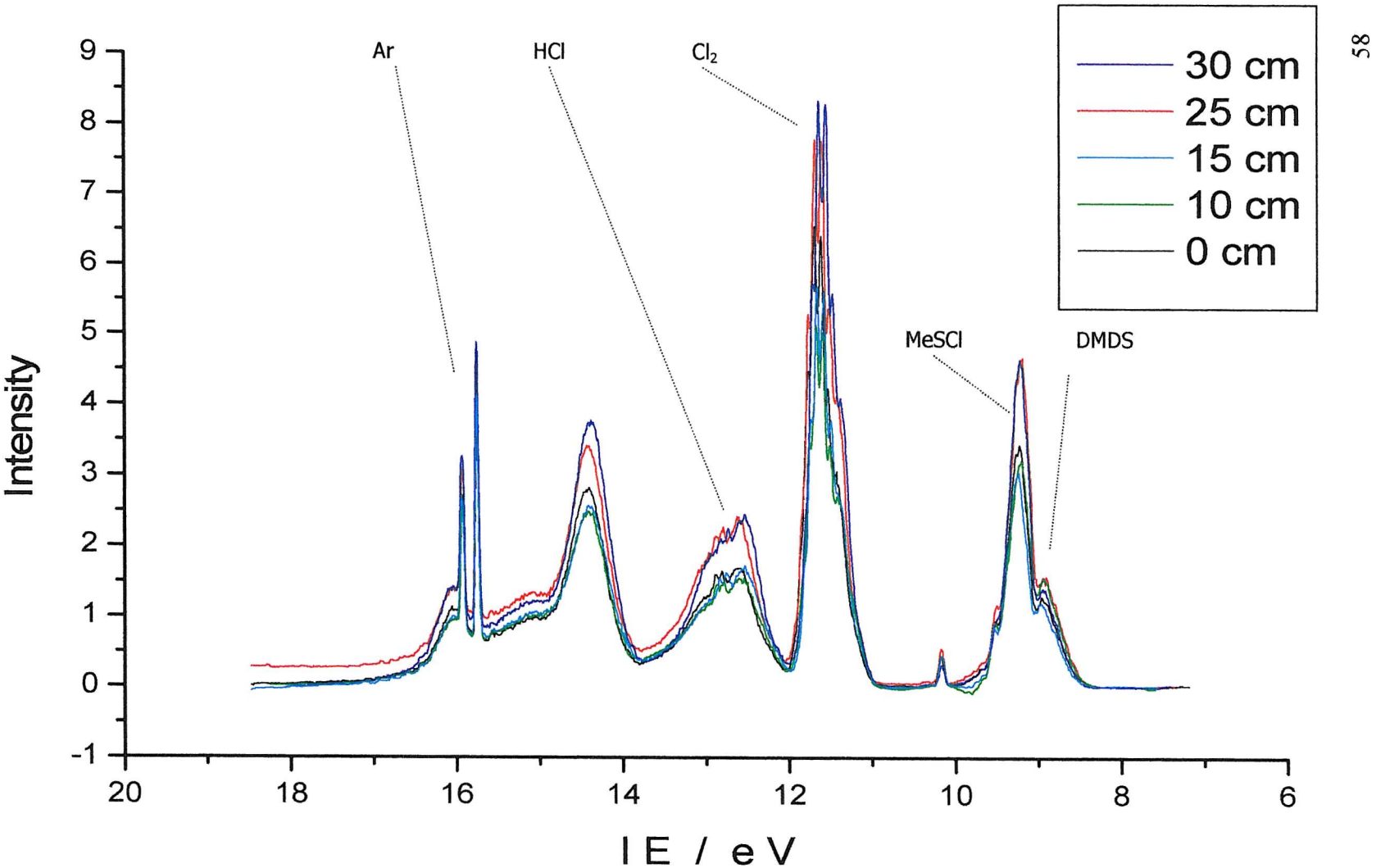

Figure 4.5: Photoelectron spectra obtained for the DMDS+Cl_2 reaction using a 1mm exit hole inlet system, recorded at different mixing distances.

On repeating the experiment with a 0.5mm exit hole inlet system the reaction goes to completion (Fig. 4.6) and only products bands are observed.

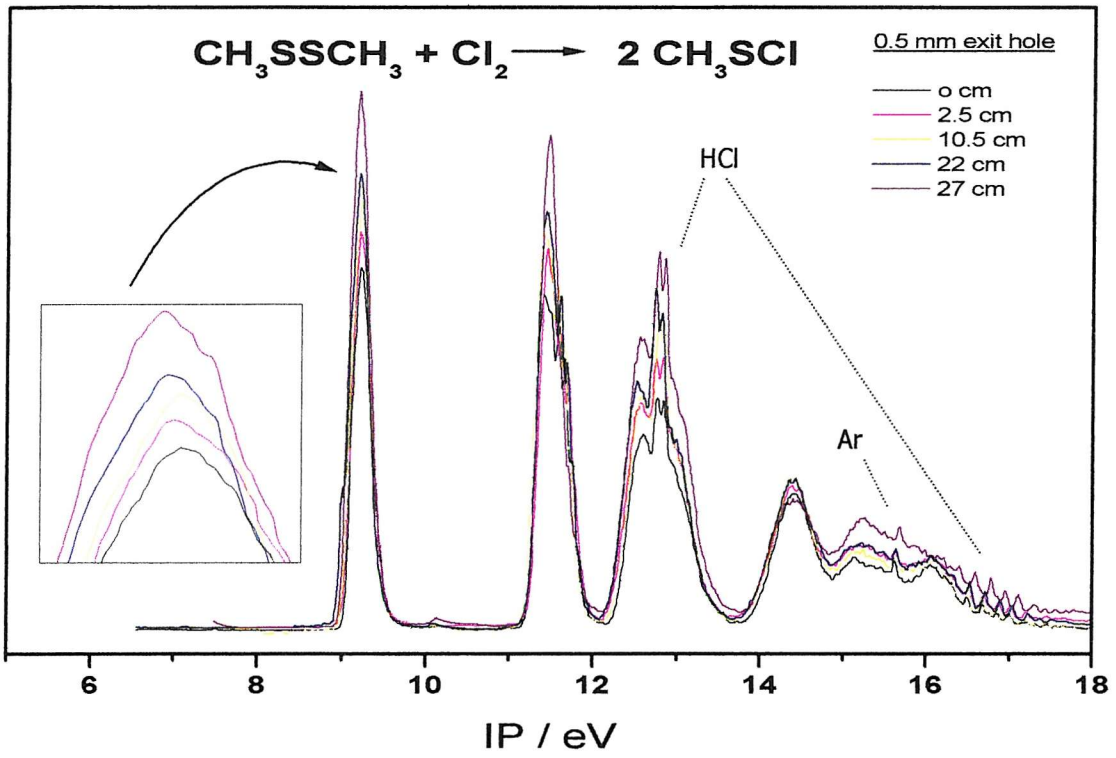

Figure 4.6: Photoelectron spectra obtained for the DMDS+Cl_2 reaction using a 0.5 mm exit hole inlet system, recorded at different mixing distances.

- **4.3 Cl + DMS Reaction.**

The DMS+Cl and DMDS+Cl reactions have been studied using two different sources of chlorine atoms: microwave discharges of silicon tetrachloride or chlorine, both mixed with argon.

Photoelectron spectra recorded for DMS, reacted with products of a $SiCl_4$/Ar discharge at several mixing distances above the photon beam, are shown in Fig. 4.7. Some bands at 9.18, 9.59 and 10.06 eV VIE, appear in the spectra and increase with the reaction time. They have been assigned with CH_3SCl [5], HClCS and CS_2 [1], [2] and [10].

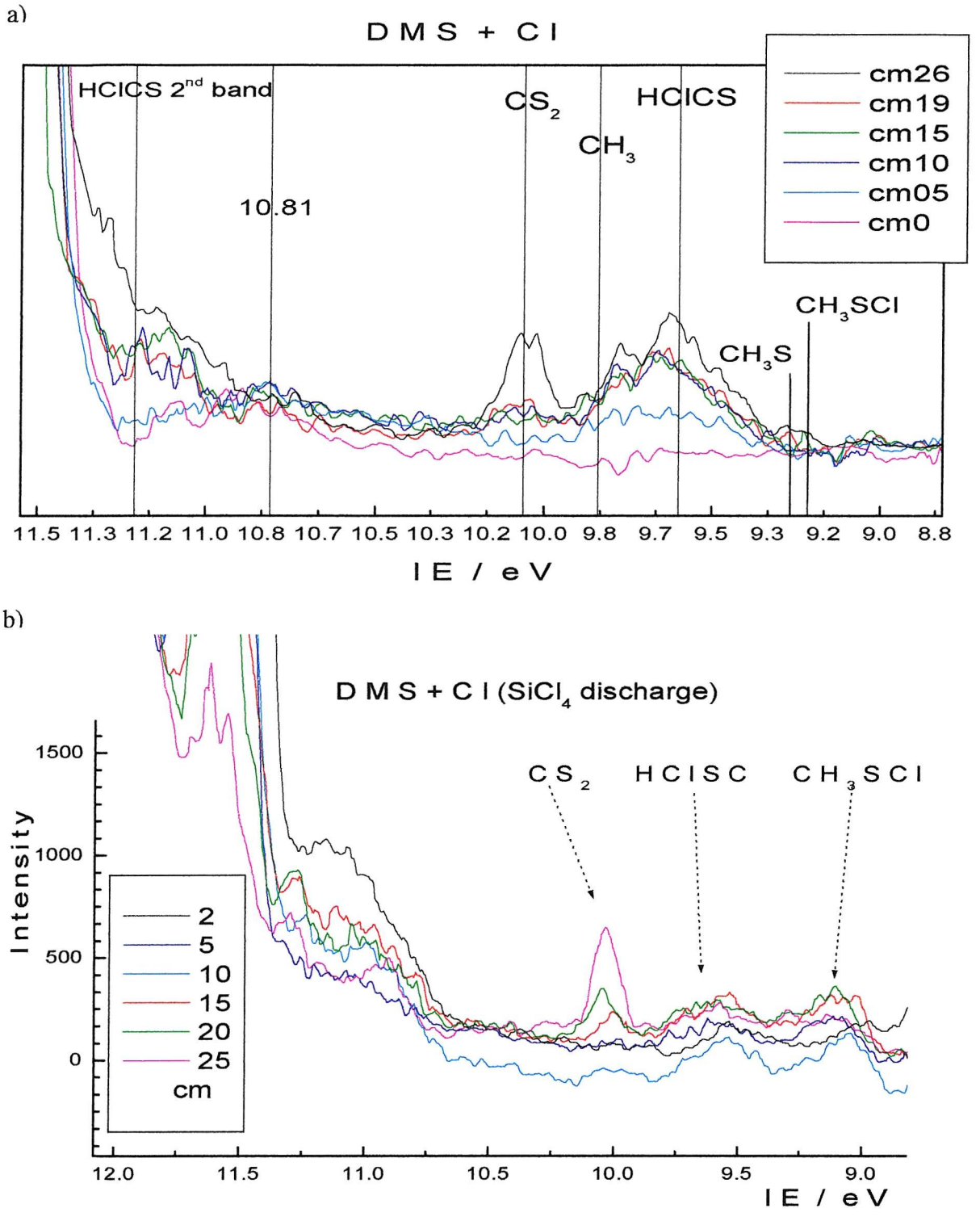

Figure 4.7: Two Photoelectron spectra recorded at different mixing distances for the Cl+DMS reaction using a $SiCl_4$ discharge to produce Cl atoms. The DMS bands have been subtracted. The difference between spectra a and b is due to the different quality of the coating tube.

The assignment of the band at 9.59 eV VIE to HClCS has been achieved from the known VIEs of Cl_2CS [12] and H_2CS [10] of 9.84 and 10.88 eV (Cl_2CS); 9.38 and 11.76 eV (CH_2S). Hence the first two VIEs of HClCS are expected at approximately 9.61 and 11.33 eV. Evidence for the second band of HClCS is the increase of a weak band around 11.21 eV VIE as the first band of HClCS increases, as can be seen in Figure 4.7a. In earlier work in the Southampton PES group, the DMS+F reaction was studied [1.16]. One of the products obtained in this case was a similar molecule, HFCS, with VIEs of 10.15, 11.49 and 13.71 eV. The weak band at 10.81 eV VIE has not been assigned yet.

Figure 4.8 shows spectra recorded for the DMS+Cl reaction using a microwave discharge of molecular chlorine in argon for different mixing distances. The first band of DMS can be seen clearly at 8.68 eV. This decreases in intensity with the reaction time. Bands associated with products from the Cl+DMS reaction overlap with the product bands from the DMS+Cl_2 reaction. The product HClCS cannot be observed. The first band of CH_3SCl overlaps with the first band of CH_3SCH_2Cl but the second band of CH_3SCl at 11.28 eV VIE [5] confirms its presence in the reaction.

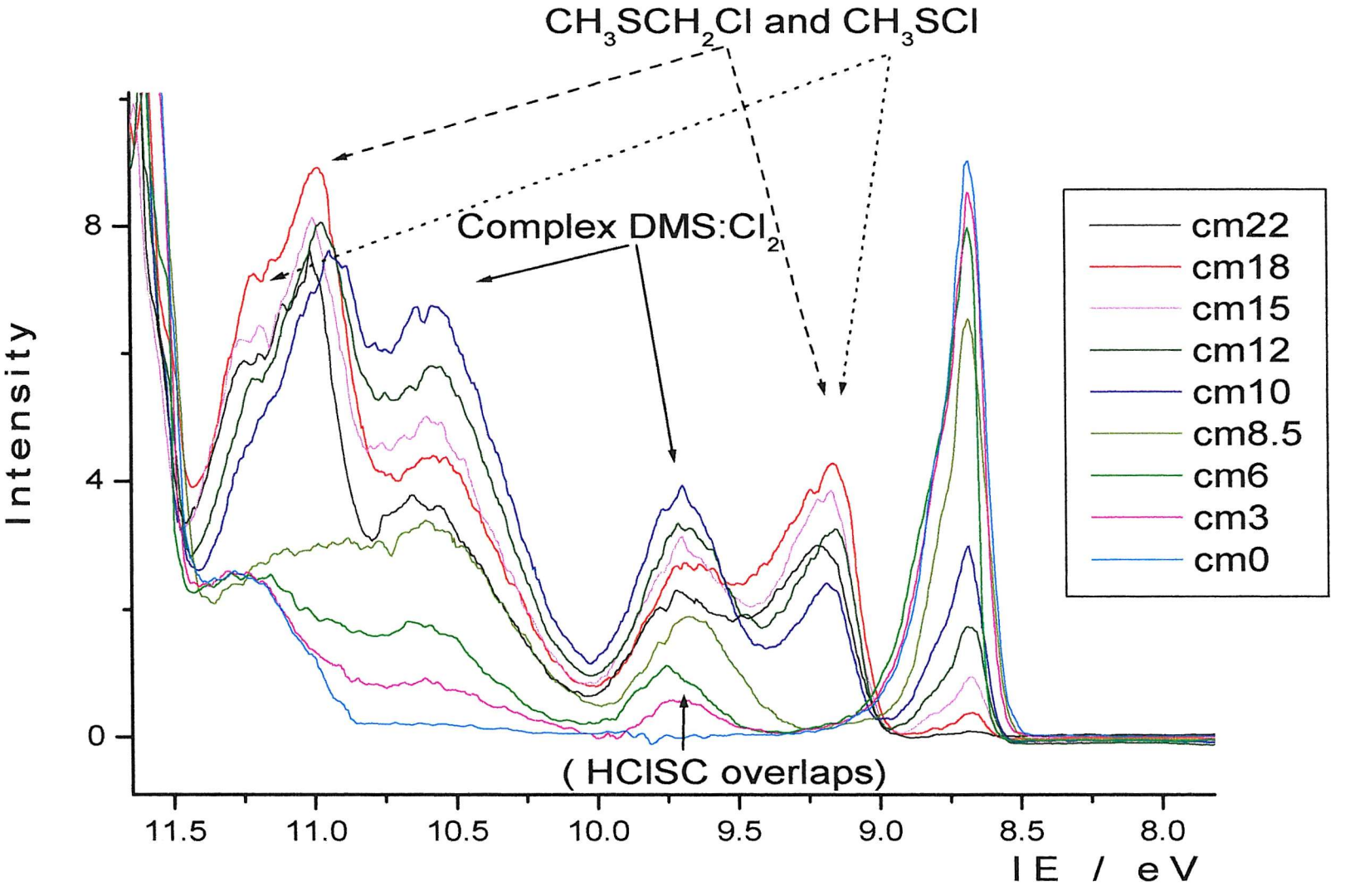

Figure 4.8: Photoelectron spectra recorded at different mixing distances for the Cl+DMS reaction, with Cl atoms produced using a Cl_2 discharge.

- **4.4 Cl + DMDS Reaction.**

Photoelectron spectra recorded for DMDS, reacted with products of a $SiCl_4$/Ar discharge at several mixing distances above the photon beam, are shown in Fig. 4.9. The first band of DMDS can be seen clearly at 8.96 eV VIE. This decreases with reaction time. Three bands at 9.18, 9.61, 10.06 eV, appear in the spectra and increase with the reaction time. They have been assigned to CH_3SCl [5], HClCS and CS_2 [1], [2] and [10].

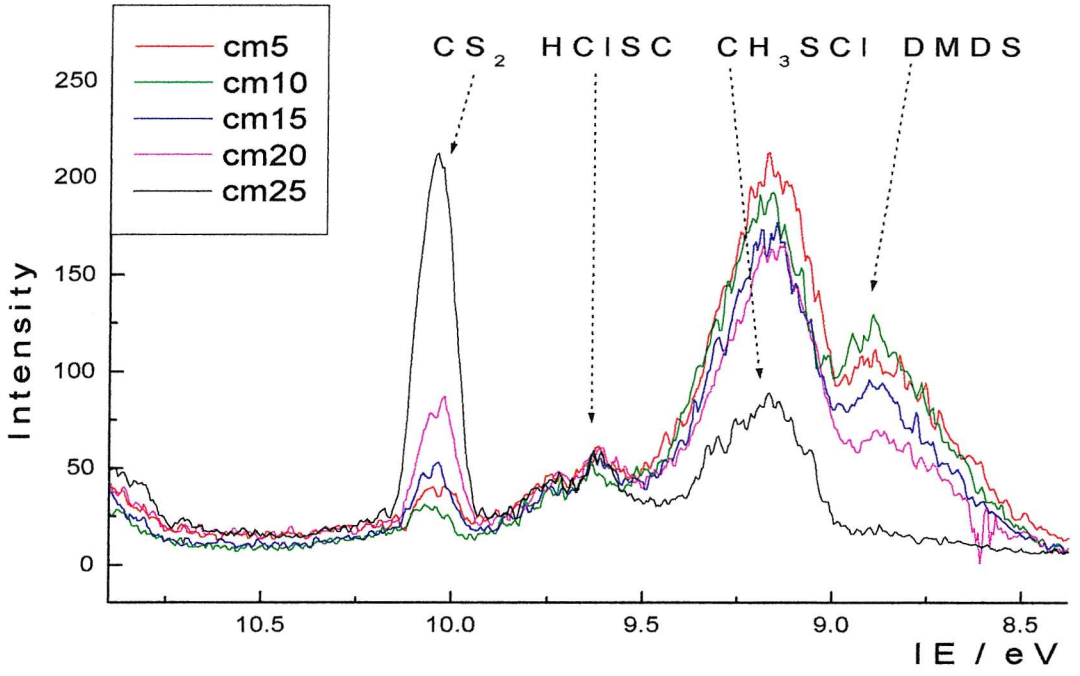

Figure 4.9: Photoelectron spectra recorded at different mixing distances for the Cl+DMDS reaction using a $SiCl_4$ discharge to produce Cl atoms.

Figure 4.10 shows photoelectron spectra recorded for the DMDS+Cl reaction using a chlorine microwave discharge to produce Cl atoms, at different mixing distances. The first band of DMDS can be seen clearly at 8.96 eV VIE. This decreases in intensity with reaction time. The product bands for this reaction are different due to the different source of chlorine atoms. The bands at 9.39, 10.06, 10.45 eV VIE have been assigned to CH_3SH [1], [2] and [6]; CS_2 and H_2S [1], [2] and [10].

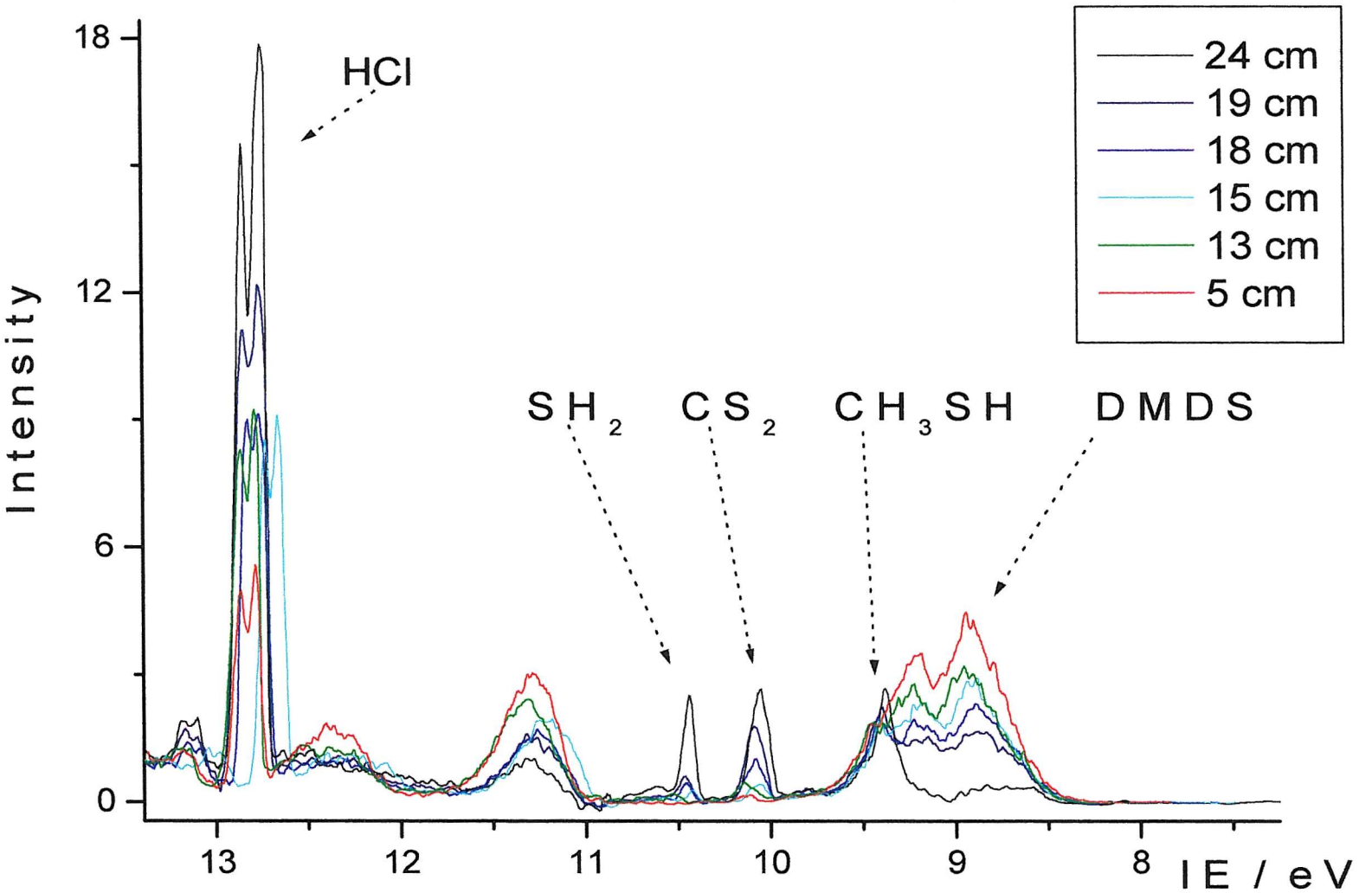

Figure 4.10: Photoelectron spectra recorded at different mixing distances for the Cl+DMDS reaction using a Cl_2 discharge to produce Cl atoms.

- **4.5 Ozone plus Ethylene.**

The final reaction studied was ethylene plus ozone. This is known to be a slow reaction with a rate constant at room temperature of 1.91×10^{-18} cm^3 $molecule^{-1}s^{-1}$. The spectrum shown in Figure 4.11 was obtained using a mixing distance of 8.5 cm and a 1mm exit hole tube. Ozone has been pumped off silica gel until a spectrum of pure ozone was obtained (containing no oxygen), the oxygen present in the spectrum is a product of reaction.

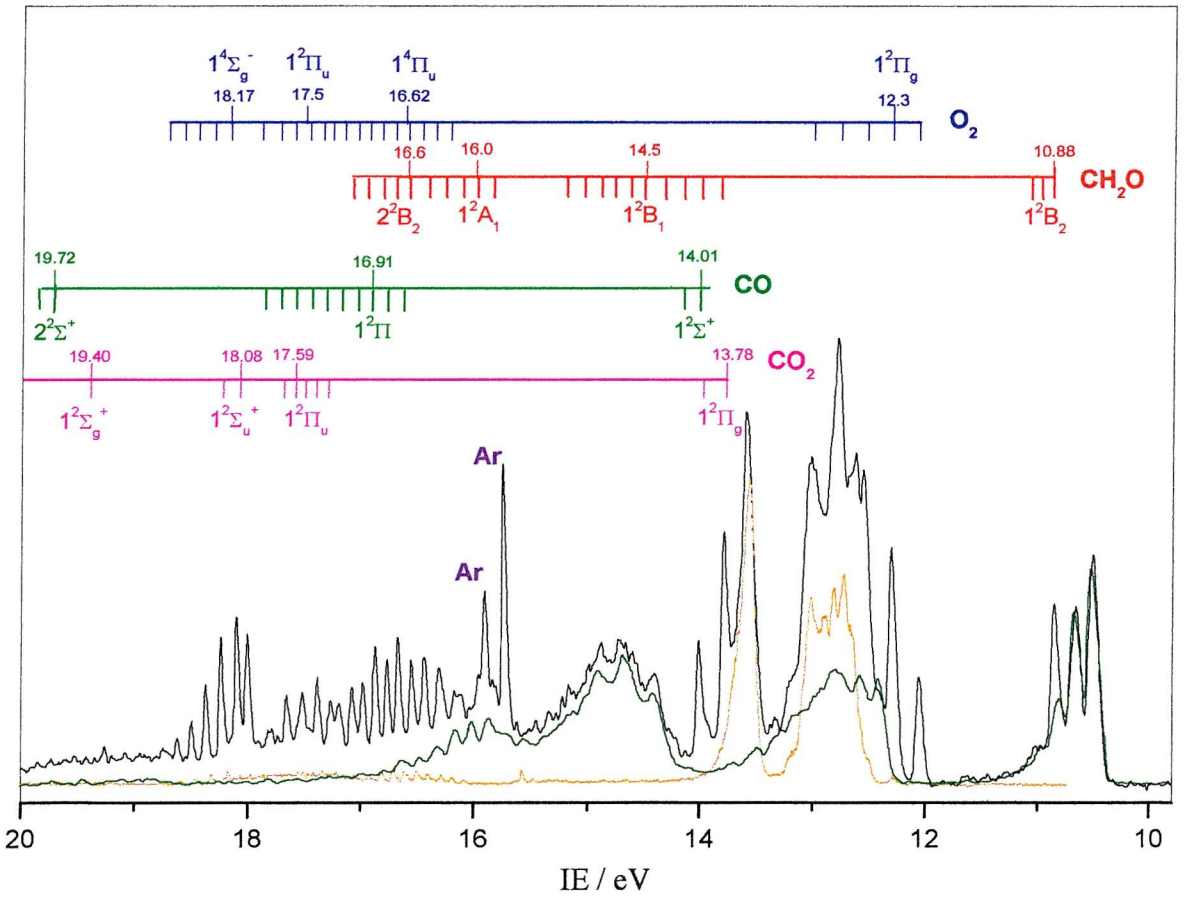

Figure 4.11: Photoelectron spectrum recorded for the O_3+ethylene reaction with a 1 mm exit hole tube. The green and orange lines correspond to ethylene and ozone respectively. On subtraction of the bands of these reactants from the spectrum, product bands can be seen i.e. bands of O_2, CH_2O, CO and CO_2.

When the reaction is carried out with a smaller exit hole tube, O_2 $^1\Delta_g$ is observed as a reaction product (Figure 4.12). Reactions of this kind, which give rise to electronically exited products are of great interest in physical chemistry, since it is more usual to find only rovibronic excitation in the products. Such systems may have applications in laser technology.

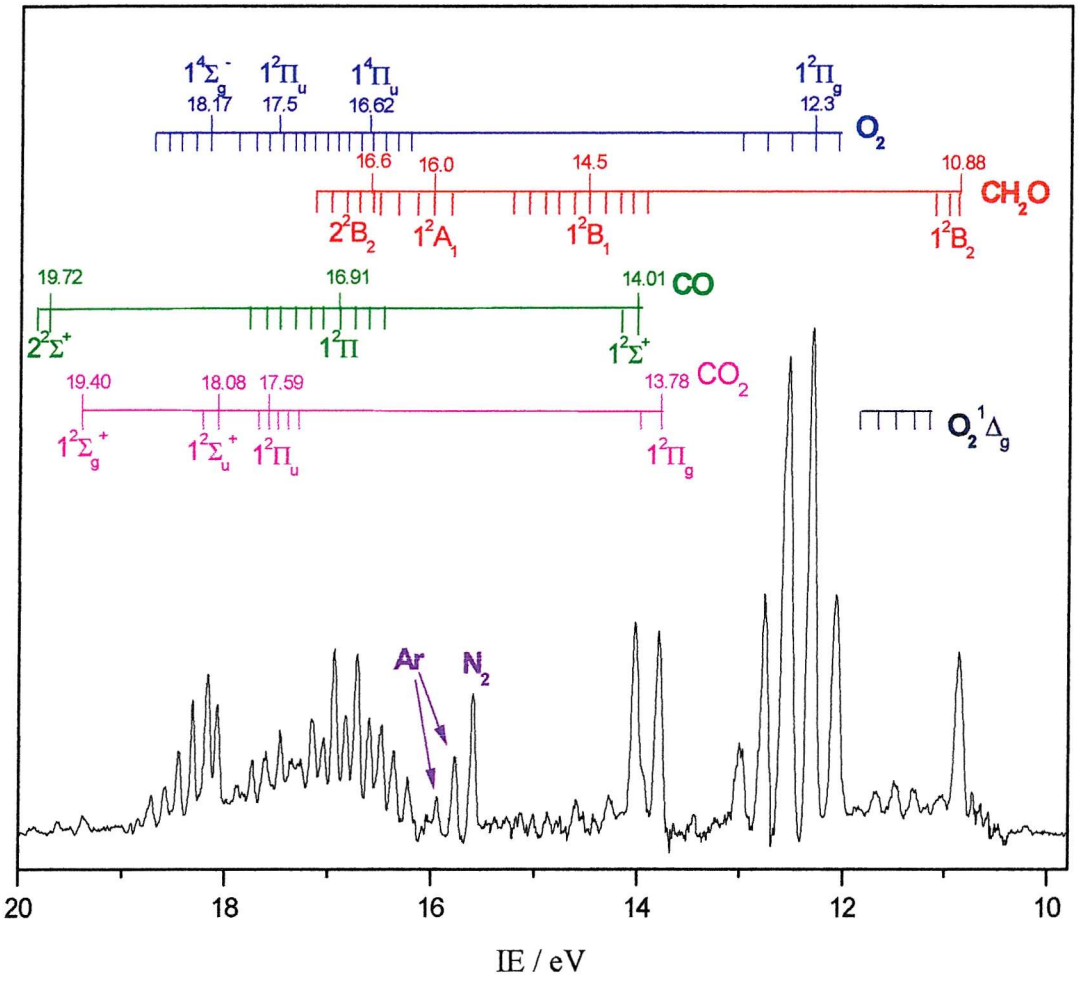

Figure 4.12: Photoelectron spectrum recorded for the O_3+ethylene reaction with a 0.5 mm exit hole tube.

Complete reaction was observed with a 0.5mm exit hole inlet system and this indicates that long reaction times are required for complete reaction. In comparison, with a new open inlet system with a very long mixing distance (≈ 3.3 m) O_2 $^1\Delta_g$ was also observed even if the reaction does not go to completion (Fig.4.13).

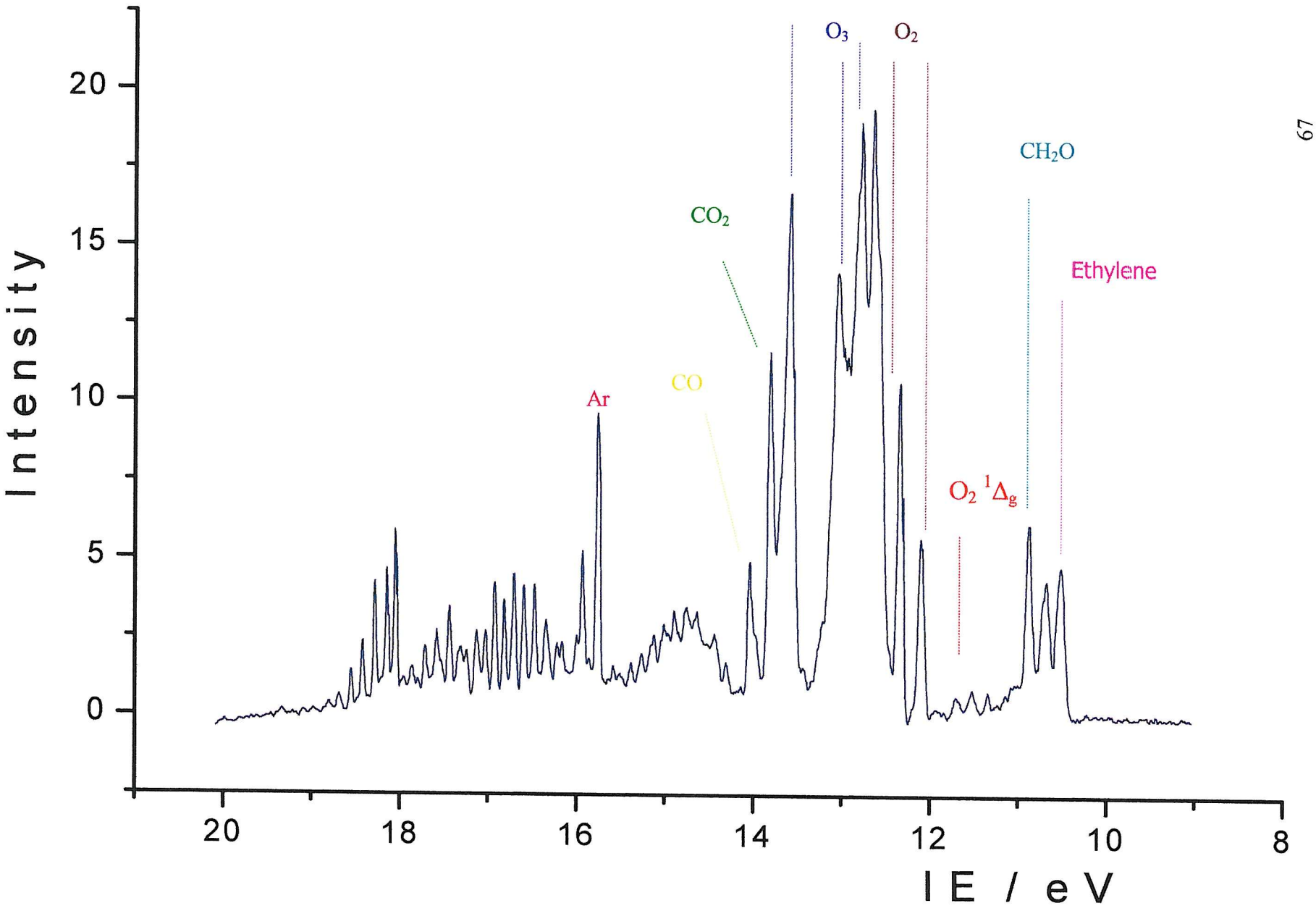

Figure 4.13: Photoelectron spectrum recorded for the O_3+ethylene reaction with a open exit hole tube with a very long mixing distance (≈ 3.3 m).

Repeating the experiment with a new inlet system allows the study of the reaction at longer mixing distance (up to 10 meter of mixing distance), with an open inlet tube of the type shown in Figure 2.8. The characteristics of this "open tube" system only allow a range of 20-40% reaction (as estimated from the ethylene first band intensity) depending of the total pressure of reactant in the system. The plot of relative intensity against the mixing distance for this reaction is shown in Figure 4.14. The inlet system was tested with 10 meter of maximum mixing distance but the reaction gave maximum products around six meters mixing distance. Modifications were carried out to adapt the maximum mixing distance to 6.3 meters and the spectra were recorded at different mixing distance. The results are shown in Figures 4.14 and 4.15.

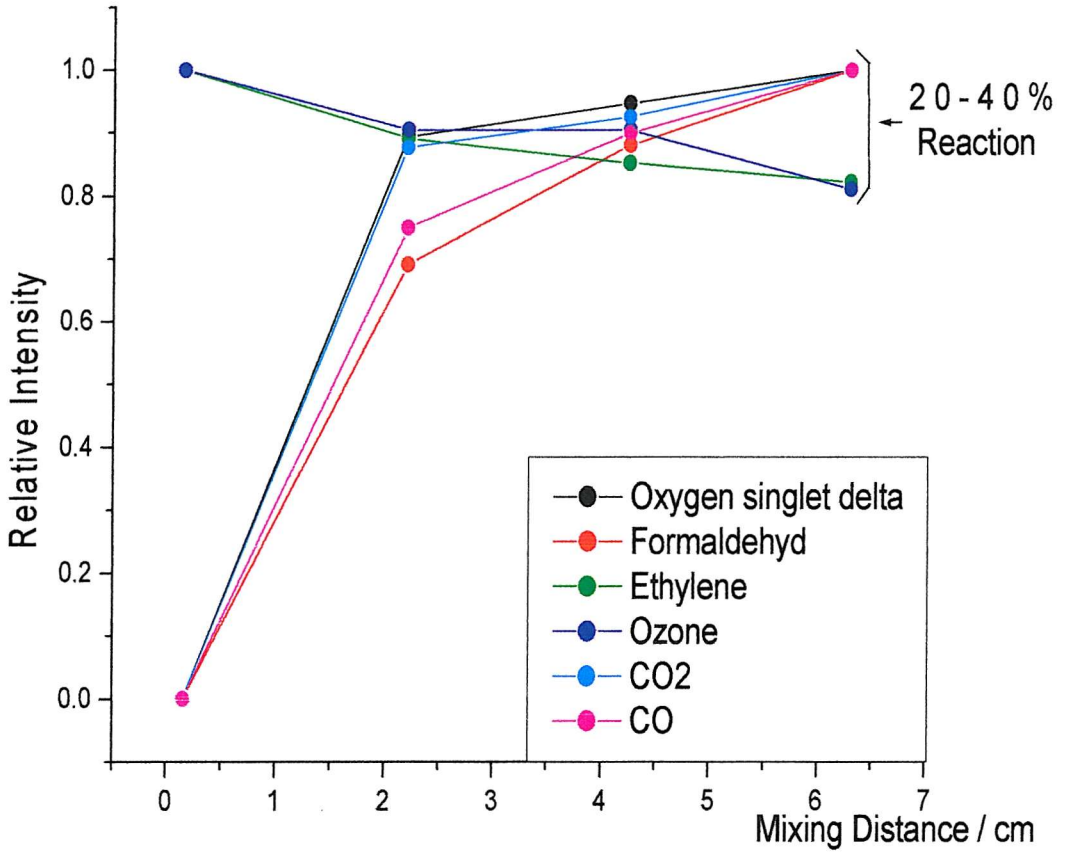

Figure 4.14: A plot of relative intensity against mixing distance for the O_3+ethylene reaction, with a open exit hole tube.

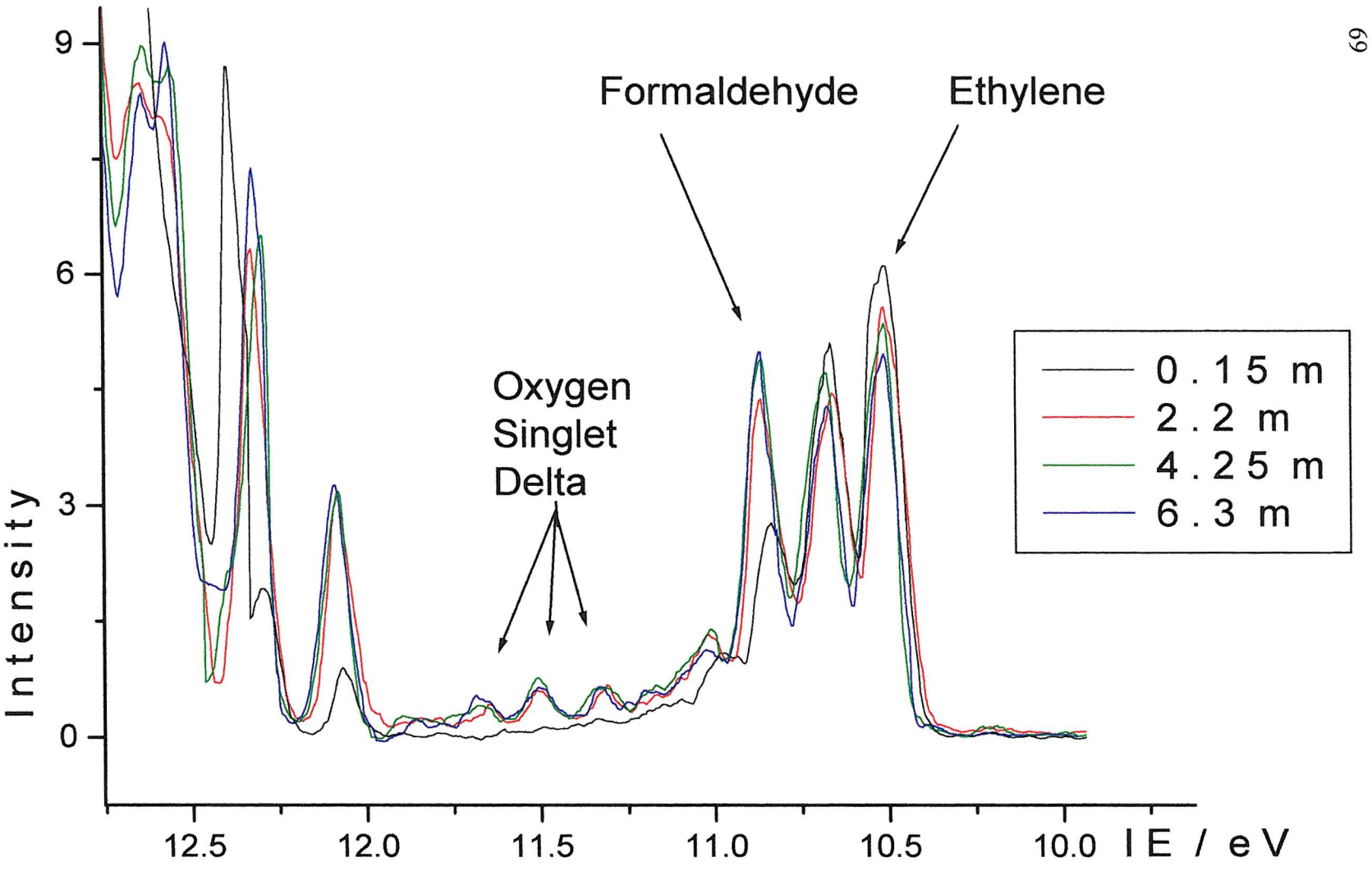

Figure 4.15: Photoelectron spectra recorded for the O_3+ethylene reaction with an open exit hole tube at several mixing distance.

CHAPTER 5.
Discussion

- **5.1 Cl_2 + DMS Reaction Mechanism.**

In the first part of this work, the reaction between DMS and Cl_2 was considered. It was found that a complex (CH_3SCH_2Cl:HCl) is formed at short reaction times (Fig. 4.1). It then decomposes to the final products, CH_3SCH_2Cl and HCl when the reaction time is increased (Fig. 4.2).

If the energy diagram of the reaction is considered, it can be seen that two kinds of complex can be proposed, a reactant complex and a product complex, as shown in Figure 5.1.

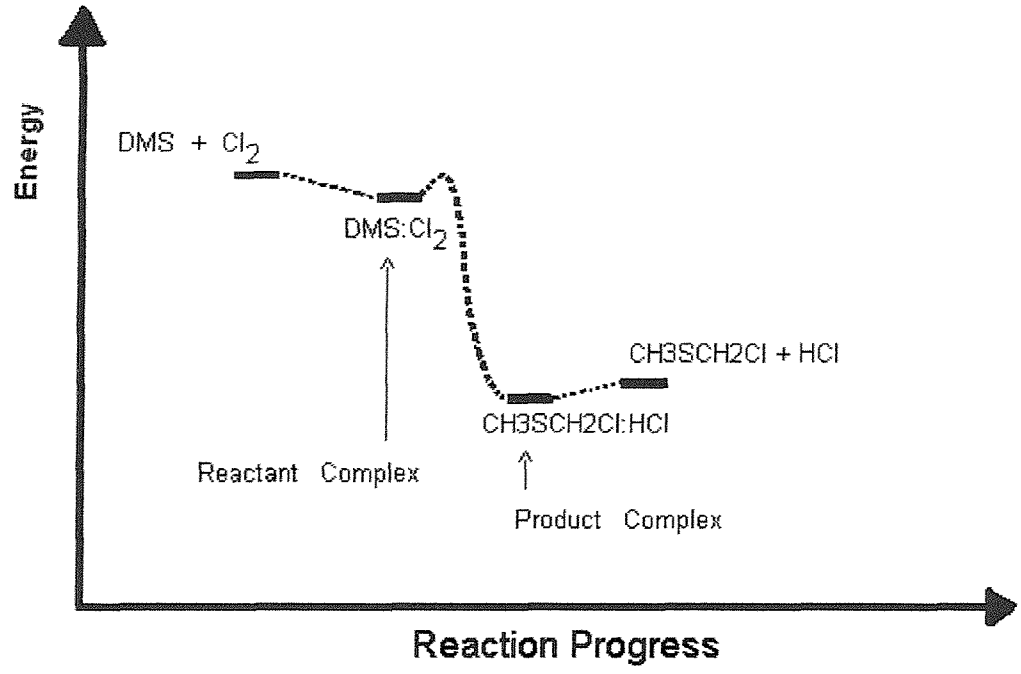

Figure 5.1: Schematic diagram of the reaction DMS+Cl_2.

At first it was thought that the observed bands associated with a reaction intermediate were corresponded to the DMS:Cl_2 complex. The relative energies of the reagents, products and intermediates shown in Figure 5.1 were not known.

Calculations of the first VIE of the complex gave 8.93 eV (based on the RCCSD / aug-cc-pVTZ value).

Methods	VIE/eV	Nbasis
MP2/aug-cc-pVDZ	8.87	181
MP2(full)/aug-cc-pVDZ	8.88	181
RCCSD/aug-cc-pVDZ	8.77	181
RCCSD(T)/aug-cc-pVDZ	8.83	181
MP2(full)/6-311++G(3df,3pd)	8.95	327
RCCSD/aug-cc-pVTZ	*8.87*	*380*
Best estimate[a]	8.93	
Experimental	9.66	

***Table 5.1**: First VIE of DMS.Cl_2 at the MP2(full)/6-31++G** geometry of the neutral (C_S)*

[a] Based on the RCCSD/aug-cc-pVTZ value, plus contribution of the triples from the RCCSD and RCCSD(T) calculations with the aug-cc-pVDZ basis set; this estimate is roughly at the RCCSD(T)/aug-cc-pVTZ level and is a lower limit, in view of the observed basis set effect.

This value differs considerly from the experimental first VIE (9.66 eV). Recent calculations on the product complex gave a VIE (9.54 eV), closer to the experimental value (Table 4.1). Also, as can be seen from Table 5.2, the total energy of the product complex was much lower than that of reactant complex. Table 5.2 shows the computed total electronic energies (E_e) and relative electronic energies (E_{rel}) of $CH_3SCH_3+Cl_2$, $CH_3SCH_3.Cl_2$, $CH_3SCH_2Cl.HCl$ and $CH_3SCH_2Cl+HCl$ at different levels of calculations.

E_e (hartrees)	$CH_3SCH_3+Cl_2$	$CH_3SCH_3.Cl_2$	$CH_3SCH_2Cl.HCl$	$CH_3SCH_2Cl+HCl$
MP2/6-311++G(3df,3pd)	-1396.69465	-1396.70774	-1396.75626	-1396.74583
RCCSD/aug-cc-pVDZ	-1396.54777	-1396.55636	-1396.60645	-1396.59967
RCCSD(T)/aug-cc-pVDZ	-1396.57313	-1396.58501	-1396.63376	-1396.62642
RCCSD/aug-cc-pVTZ	-1396.81180	-1396.81865	-1396.86324	-1396.85603
E_{rel} (kcal.mole^{-1})				
MP2/6-311++G(3df,3pd)	0.0	-8.2	-38.7	-32.1
RCCSD/aug-cc-pVDZ	0.0	-5.4	-36.8	-32.6
RCCSD(T)/aug-cc-pVDZ	0.0	-7.5	-38.0	-33.4
RCCSD/aug-cc-pVTZ	0.0	-4.3	-32.3	-27.8
RCCSD(T)/aug-cc-pVTZ[a]	0.0	-6.4	-33.5	-28.6
ZPVE[b] (kcal/mole)	48.5	50.3	49.2	46.7
Rel. (E_e + ZPVE)[c] (kcal/mole)	0.0	-4.6	-32.8	-30.0

Table 5.2: Computed total electronic energies (E_e) and relative electronic energies (E_{rel}) of $CH_3SCH_3+Cl_2$, $CH_3SCH_3.Cl_2$, $CH_3SCH_2Cl.HCl$ and $CH_3SCH_2Cl+HCl$ at different levels of calculations.

[a] Taking the triple contributions from the aug-cc-pVDZ basis set.

[b] Vibrational frequencies from B3LYP/6-31G** calculations for CH_3SCH_3 and CH_3SCH_2Cl, experimental vibrational frequencies for HCl and Cl_2 and MP2/6-31++G** vibrational frequencies for the two complexes.

[c] RCCSD(T)/aug-cc-pVTZ E_{rel} + ZPVE correction (at 0 K).

The most stable geometry of the complex CH_3SCH_2Cl:HCl has C_1 symmetry, as shown in Figure 5.2.

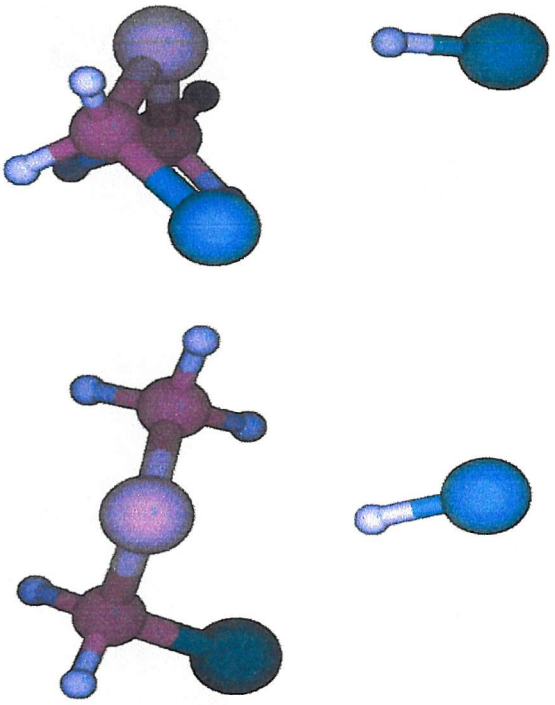

MP2/6-31++G**
E_e=-1396.4106417 hartrees

Geometry optimization and harmonic frequency calculations

MP2/6-31++G** lowest minimum structure: C_1

{MP2(full)/6-31++G** gave an almost identical geometry}

Optimized geometrical parameters (in Å and °):

SC=1.806, SC_1=1.793, C_1Cl=1.789, HCl=1.282, S...H=2.467;

CSC_1=99.30, SC_1Cl=114.82, S...HCl=163.86

Figure 5.2: Schematic picture from two different directions of the most stable geometry for the complex CH_3SCH_2Cl:HCl and some structural parameters obtained by *ab initio* calculations.

From the relative band intensities measured from the photoelectron spectra recorded for the reaction DMS+Cl_2, at different mixing distances at constant reagent partial pressure, it can be seen that the complex is formed at intermediate reaction times but it decomposes at later times to give CH_3SCH_2Cl+HCl. This plot is shown in Figure 4.3.

This reaction can be written as:

$$\mathbf{DMS + Cl_2 \rightarrow (CH_3SCH_2Cl{:}HCl) \rightarrow CH_3SCH_2Cl + HCl} \qquad (5.1)$$

Given the relative energies, listed in table 5.2, it would be useful to test this proposed assignment by studying the reaction $HCl+CH_3SCH_2Cl$ by PES to observe bands associated with the $CH_3SCH_2Cl{:}HCl$ intermediate.

- **5.2 Cl_2 + DMDS Reaction Mechanism.**

Figure 4.5 shows spectra recorded for the DMDS+Cl_2 reaction, using a 1mm exit hole inlet system, recorded at different mixing distances. As can be seen, the reaction is not complete even at the longest mixing distance. Two products are detected, CH_3SCl and HCl.

On repeating the experiment with a 0.5mm exit hole inlet system, the reaction goes to completion (Fig. 4.6) and only products bands are observed.

The mechanism can be written as:

$$\mathbf{DMDS + Cl_2 \rightarrow CH_3SCl^*} \begin{cases} \rightarrow \mathbf{CH_3SCl} \\ \rightarrow \mathbf{H_2CS + HCl} \end{cases} \qquad (5.2)$$

(Vibrationally excited)

The H_2CS first band (1^{st} VIE 9.34 eV [10]) overlaps with the CH_3SCl first band (1^{st} VIE 9.21 eV [5]), and the H_2CS second band(1^{st} VIE 11.78 eV [10]) overlaps with the molecular chlorine first band (1^{st} VIE 11.59 eV [1]). However the presence of HCl, which increases with reaction time, supports the suggested mechanism.

• 5.3 Cl + DMS Reaction Mechanism.

In the case of the DMS+Cl reaction, the experimental evidence suggests two possible pathways. In the first, the first step is hydrogen abstraction which produces the unstable radical CH_3SCH_2. Further reaction with Cl or Cl_2 gives rise to either HCl, CH_3 and HClCS. The second channel gives directly CH_3SCl and the radical CH_3.

The different results obtained with the two discharge sources of chlorine atoms (Figure 4.7 and 4.8) arise because of the different relative partial pressures of molecular chlorine and atomic chlorine produced in the two methods. In a molecular chlorine discharge the amount of molecular chlorine present during reaction is much bigger (and the Cl atoms partial pressure lower) than for the silicon tetrachloride discharge; consequently the products of reaction with molecular chlorine are present with those of atomic chlorine in the Cl+DMS reaction where Cl is produced from a Cl_2/Ar discharge.

The suggested pathways can be summarized as follows:

Microwave discharge on $SiCl_4$ or Cl_2

Route 1 $\quad DMS + Cl \rightarrow HCl + CH_3SCH_2$

$\quad + Cl_2$

$\quad HCl + CH_3 + HClCS$

Route 2 $\quad DMS + Cl \rightarrow CH_3SCl + CH_3 \qquad (5.3)$

- **5.4 Cl + DMDS Reaction Mechanism.**

In the case of the reaction of DMDS with Cl there are also two reaction channels. The first one gives rise to CH_3SCl and the unstable radical CH_3S which then reacts rapidly with DMDS or Cl_2 to give CH_3SH or CH_3SCl respectively. This is similar to the DMS plus Cl case, where in the first channel the unstable radical reacts with Cl_2 producing HCl, HClCS and CH_3S which again reacts with DMDS or Cl_2 to give CH_3SH and/or CH_3SCl. Again a $Ar/SiCl_4$ discharge gives a larger amount of chlorine atoms than a Cl_2/Ar discharge.

The different pathways of this reaction are:

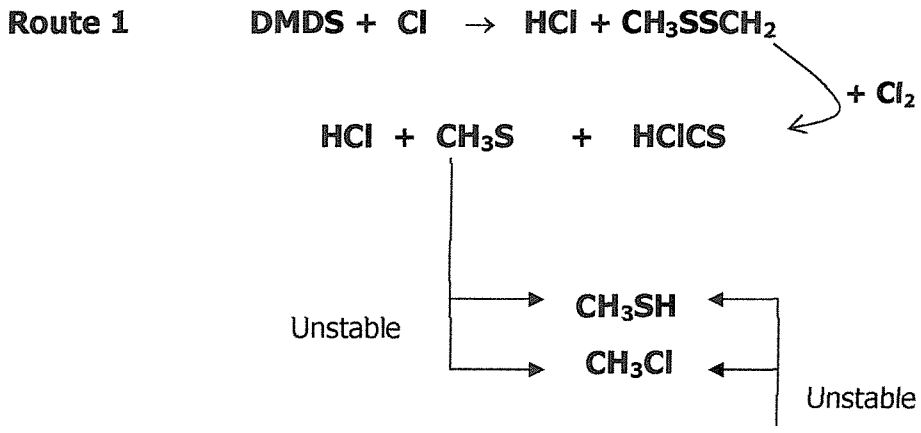

The next step in this project, which involves performing kinetic studies, will be described in the next chapter.

- **5.5 Ozone+Ethylene Reaction Mechanism.**

The final reaction studied is ethylene plus ozone. Both, alkenes and ozone are found in the atmosphere, with alkenes showing increased partial pressures in the regions of pine forests.

Laboratory measurements have shown that OH radicals are generated in reactions with alkenes; however the exact nature of the mechanism of the reaction is not properly understood.

Theoretical work has suggested that this reaction involves first the formation of a primary ozonide which can then either rearrange to a second ozonide or can break down further to produce formaldehyde and a excited Criegee intermediate [13-18], as shown in Figure 5.3.

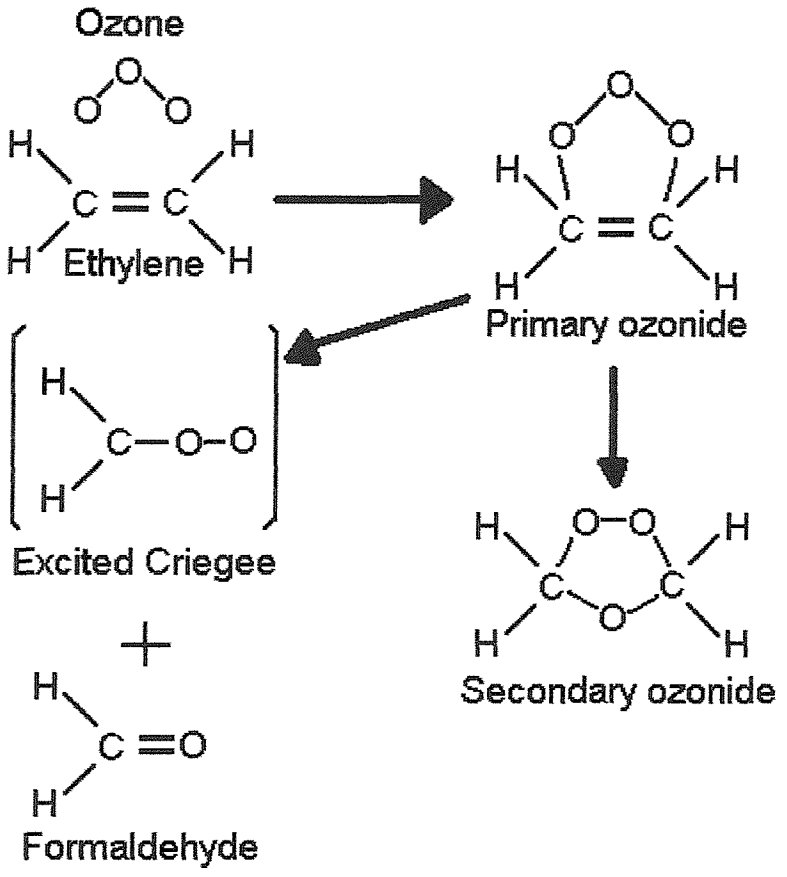

Figure 5.3: Schematic mechanism of the ozone+ethylene reaction.

The results obtained in this work are consistent with this overall mechanism but the intermediates (notably the Criegee intermediate) has not been observed. However, observation of bands associated with O_2 $a^1\Delta_g$ seems consistent with the Criegee intermediate reacting with O_3 to give this product.

The excited singlet delta of oxygen ($a^1\Delta_g$ O_2) can be produced by a microwave discharge of oxygen and differs in energy with the ground state ($X^3\Sigma_g$ O_2) by approximately 1 eV, so an energetic process is necessary to form it. The presence of this excited state of oxygen from the reaction of ozone with ethylene may be explained by the reaction of the excited Criegee with ozone, to form formaldehyde and either two molecules of singlet delta oxygen or two oxygen molecules in the triplet sigma state, as shown in Figure 5.4. These should be possible because the reactions are very exothermic and the total spin angular momentum of the reaction is conserved, as shown in Figure 5.5.

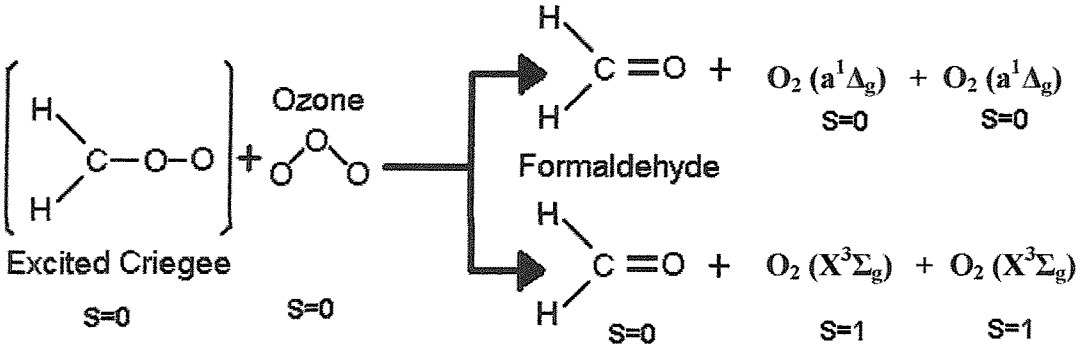

Figure 5.4: Schematic mechanism of the reaction of the excited Criegee with ozone.

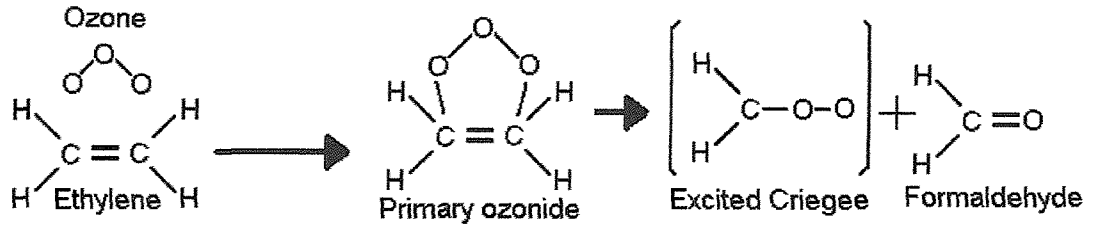

Max ΔH = -21.3 Kcal/mol = -0.92 eV

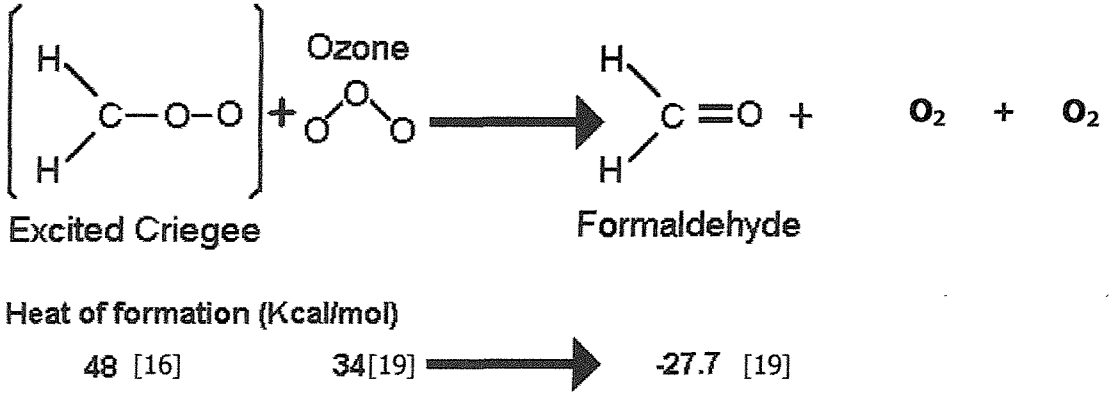

Max ΔH = -133.7 Kcal/mol = -5.78 eV

Figure 5.5: Schematic diagram showing the heats of the reactions of ozone plus ethylene and the Criegee intermediate with ozone.

The next step in this project in order to obtain more evidence of these pathways will be described in the next chapter.

- **5.6 References.**

[1] *"Handbook of HeI Photoelectron Spectra of Fundamental Organic Molecules"*
By K. Kimura, S. Katsumata, Y. Achiba, T. Yamazaki and S. Iwata
Japan Scientific Societies Press, Tokyo (1981)
Halsted Press, New York.

[2] *"Molecular Photoelectron Spectroscopy, A Handbook of He 584 Å Spectra."*
D. W. Turner, C. Baker, A. D. Baker and C. R. Brundle.
Wiley-Interscience, a division of John Wiley and Sons Ltd.

[3] J.M. Dyke, N. Jonathan, E. Lee and A. Morris.
J. of the Chemical Society, Faraday Transactions II, Vol. **72** (1976).

[4] B. Ruscic and J. Berkowitz: Photoionization of CH_2S and HCS.
J. Chem. Phys., Vol. **98**, No. 4, 15 February 1993

[5] E. Nagy-Felsobuky and J. Barrie Peel.
Phosphorus and Sulfur, Vol. **7** (1979)pp. 157-160

[6] J. M. Nicovich, K. D. Kreutter, C. A. van Dijk and P. H. Wine.
J. Phys. Chem. **96** (1992) 2518-2528.

[7] J. Baker and J. M. Dyke.
Chem. Phys. Lett. **213**, No. 3-4 (1993) 257-261.

[8] J. Baker and J. M. Dyke.
J. of Physic. Chem. Vol. **98**, No. 3 (1994) 757-764.

[9] Bing-Ming Cheng and Eh Piew Chew; Jen-Shiang K. Yu and Chin-hui Yu.
J. of Chem. Physic. Vol. **114**, No. 11, 15 March 2001, 4817-4823.

[10] H. W. Kroto and R. J. Suffolk.
Chem. Phys. Lett. **15**, no. 4, (1972) 545-548.

[11] B. Cheng, E. P. Chew, J. K. Yu and C. Yu.
*J Chem. Phys.***114**, No. 11 (2001) 4817-4823.

[12] Chadwick, D.; Cornford, A. B.; Frost, D. C.; Herring, F. G.; Katrib, A.; McDowell, C. A.; McLean, R. A. N. *Photoelectron spectra of some dihalocompounds.* Electron Spectrosc., Proc. Int. Conf. (1972), Meeting Date 1971, 453-69. CODEN: 25QKA7 CAN 77:146043 AN 1972:546043 CAPLUS. Pag 453-470

[13] J. Baker, S. M. Aschmann, J. Arey, Roger Atkinson.
Int. J. Chem. Kinetics, **34**, (2002) 73-85.

[14] D. Johnson, A. G. Lewin and G. Marston.
J. Phys. Chem. A, **105**, (2001) 2933-2935.

[15] J. M. Anglada, R. Crehuet and J. M. Bofill.
Chem. Eur. J. ***5***, (1999) 1809-1822.

[16] W. R. Wadt and W. A. Goddard III
J. Amer. Chem. Soc. **97:11**, (1975) 3004-3021.

[17] P. C. Hiberty
J. Amer. Chem. Soc. **98:20**, (1976) 6088-6092.

[18] P. C. Hiberty and J. D. Devidal.
Tetrahedron, **35**, (1979) 1015-1017.

[19] "Handbook of Chemistry and Physics"
57th Edition, CRC Press, Inc. (1976-1977).

CHAPTER 6.
Conclusion

- **6.0 Conclusions.**

- In summary, the reactions Cl+DMS, Cl+DMDS, Cl_2+DMS and Cl_2+DMDS have been studied in this work with UV photoelectron spectroscopy. In each case, by recording spectra at different reaction times, it has been possible to monitor the primary and secondary reaction products at different stages of the reaction and hence to propose a reaction mechanism. Photoelectron bands associated with the 1:1 complex of CH_3SCH_2Cl:HCl and HClCS have been observed for the first time , and their assignment has been assisted by the results of *ab-initio* molecular orbital calculations.

The next steps in this project are to build a flow system attached to a photoelectron spectrometer to identify the reaction intermediates with photoionization mass spectrometry (PIM) and photoelectron spectroscopy, and to investigate the kinetics of these reactions.

- In the case of the reaction of ozone with ethylene, the observation of singlet delta oxygen as a reaction product is consistent with the presence of the Criegee Intermediate in its singlet state.

The reaction of ozone with ethylene is very slow ($k_{298}=1.91x10^{-18}$ $cm^3molecules^{-1}s^{-}1$) [1], but the reaction with 2,3 dimethyl 2-butene is faster ($k_{298}=$ $1.51x10^{-15}$ $cm^3molecule^{-1}s^{-1}$) [1]. In the future, the reaction O_3 + 2,3 dimethyl 2-butene will be studied by PES to gain more evidence of the involvement of a Criegee intermediate.

- **6.1 References.**

[1] S. M. Japar, C. H. Wu and H. Niki.
J. Phys. Chem. **78** (1974) 2318

CHAPTER 7.

Estimation of the Beta Parameter for Dimethyl Sulfide at $h\upsilon$= 21.22eV

- **7.0 Introduction.**

An objective of this project is to estimate the photoelectron cross-section for a molecule (e.g. DMS) in order to estimate its partial pressure from a PES signal. The aim is to compile a list of photoionization cross-sections at the HeI photon energy of all the reagents and products investigated in this work in order to estimate their partial pressures in the reactions studied.

In most photoelectron spectrometers (like the one used in this work), the radiation source is unpolarized. The intensity of a photoelectron band for an unpolarized photon beam, at a given detection angle, is related to the cross-section of the species involved by the formula, ([1-3]):

$$I_j \alpha d\sigma_j/d\Omega = (\sigma_j/4\pi) \{1 - (\beta_j/4) (3\cos^2\theta'-1)\} \quad (7.1)$$

In this formula, θ' is the angle between the direction of the electrons detected and the direction of the photon beam, σ_j is the total cross-section integrated over all angles and β is the anisotropy parameter.

As the detection angle used in the photoelectron spectrometer in the Southampton PES group is 90 degrees with respect to the photon beam, equation (7.1) can be modified to:

$$I_{j\perp} = (\sigma_j/4\pi) \{1 + (\beta_j/4)\} \quad (7.2)$$

When the photon source is polarized [3, 4], equation (7.1) is replaced by:

$$I_j \alpha d\sigma_j/d\Omega = (\sigma_j/4\pi) \{1 - (\beta_j/2) (3\cos^2\theta-1)\} \quad (7.3)$$

In this equation, θ is the angle of observation measured from the direction of the electric vector of a plane-polarized photon beam.

Hence to convert photoelectron intensities on a spectrometer using an unpolarized photon source, into relative partial pressures values, cross-section values are needed at 90° (i.e. σ_j and β are both required).

For this reason, estimation of the asymmetry parameter, β, for the first two bands of DMS has been performed using polarized radiation at $h\upsilon$=21.22 eV. This was carried out at the Elettra synchrotron (Trieste, Italy) by Ms. L. Zuin and Mr F. Innocenti of the Southampton PES group, by recording the spectra at two different angles.

- **7.1 Results.**

The spectra of DMS mixed with nitrogen, as a calibrant, have been recorded at Elettra, at two different angles of detection (0° and 60° with respect to the direction of polarization of the photon source and constant partial pressures. These spectra can be seen in Figure 7.1.

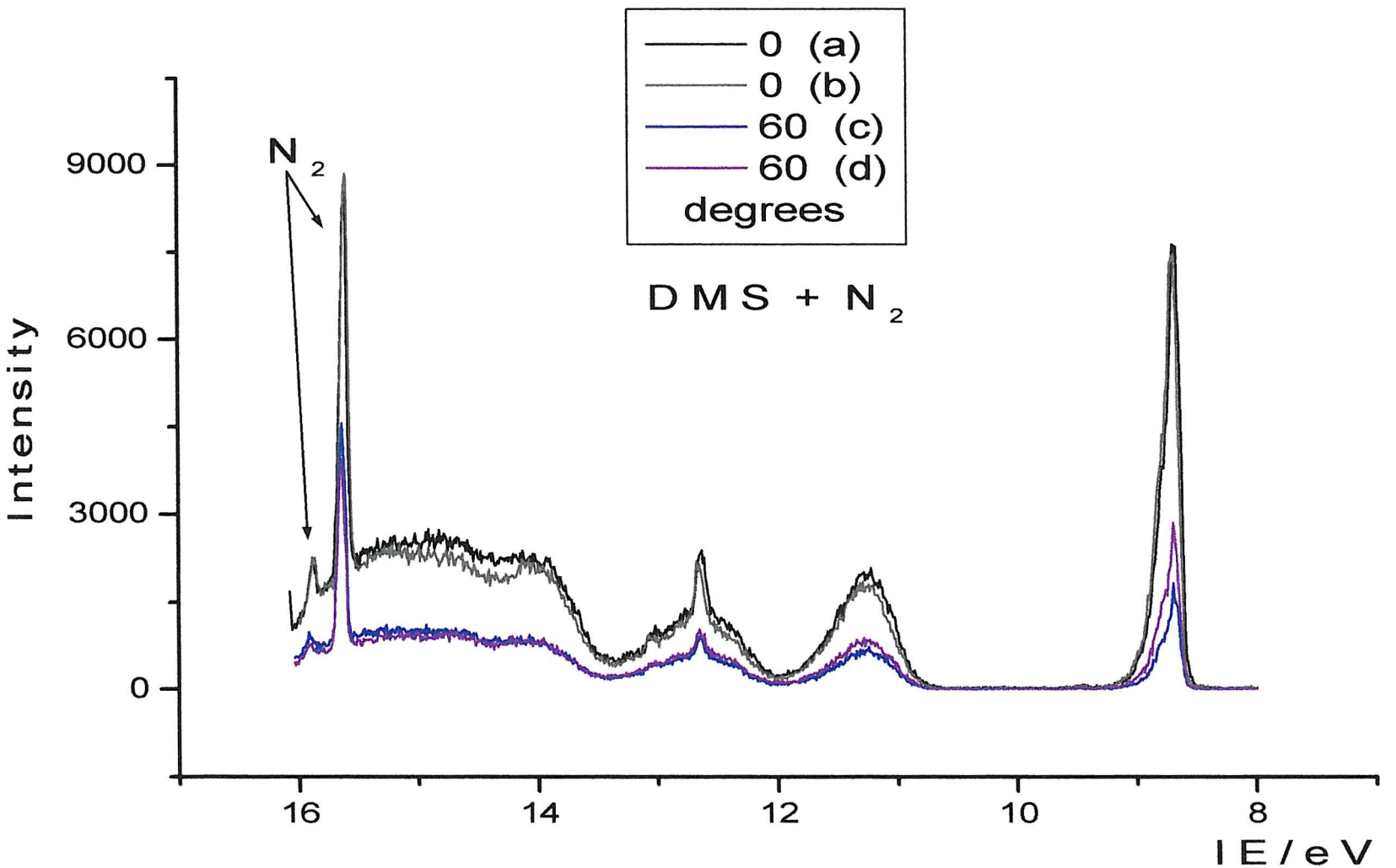

Figure 7.1: Photoelectron spectra of a mixture of DMS and nitrogen recorded using synchrotron radiation at 21.22 eV photon energy.

A correction factor must be applied to avoid systematic errors, notably associated with slight misalignment of the photon source on rotation of the hemispherical analyser and lens system. The nitrogen first band has been used for this calculation. In order to obtain the correction factor the ratio of the signal intensities, for the first N_2 band at 0 and 60 degrees, has been measured. This ratio is:

$$R = \text{Intensity}_0 / \text{Intensity}_{60} = 2.1 \qquad (7.4)$$

From equation (7.5), the experimental asymmetry parameter for N_2 can be obtained [4].

$$\beta_{N2} = 8(R-1)/(R+8) = 0.87\ \beta\text{experimental} \qquad (7.5)$$

By dividing this experimental value by the established literature value (β_{N2} first band = 0.68±0.05, [5]), the correction factor can be evaluated.

$$\text{Correction Factor} = \beta_{N2\ exp} / \beta_{N2\ th} = \mathbf{0.78} \qquad (7.6)$$

The estimation of the beta parameter for the first band of DMS is now considered. By taking the areas at different angles for the first band of DMS(Table 7.1), the experimental beta value can be estimated using equation (7.5).

Angle	Spectrum	Area	average
0°	A	1422.84	*1420.8*
	B	1418.76	
60°	C	297.78	*394.9*
	D	492.07	

Table 7.1: Areas for the first band of DMS at two different angles from Figure 7.1.

The experimental beta value for the first band of DMS is 1.79. Multiplying this value by the correction factor, the beta parameter for the first band of DMS is obtained as 1.39 i.e.

$$\beta_{DMS} = \beta_{DMS\,exp} \text{ x correction factor} = 1.79 \text{ x } 0.78 = \mathbf{1.39} \qquad (7.7)$$

To estimate the error associated with this value [6], equation (7.8) must be apply:

$$d\beta/dR = \{ [\, 8/(R+8)] - [\, 8\,(R-1) / (R+8)^2] \,\} \qquad (7.8)$$

The error in β was calculated from the error in R as 0.11. Now the recommended beta parameter is:

$$\beta_{\text{for the first band of DMS}} = \mathbf{1.39 \pm 0.11} \qquad (7.9)$$

If this value is compared with the beta parameter for the first band of H_2S at $h\upsilon$=21.22 eV (β = 1.60±0.03, [7]), it can be seen that the two values are close to each other. This is reasonable as the first bands of H_2S and DMS both correspond to ionization from a 2p lone pair on the sulfur atom.

The estimation of the beta parameter for the second band of DMS now is considered. By taking the areas at different angles for the second band of DMS (Table 7.2), the experimental beta value can be estimated by equation (7.5).

Angle	Spectrum	Area	average
0°	A	1201.98	*1122.13*
	B	1042.28	
60°	C	390.59	*439.48*
	D	488.38	

Table 7.2: Areas for the second band of DMS at two different angles from Figure 7.1.

The experimental beta value for the second band of DMS results in 1.17. Multiplying this value for the correction factor, the beta parameter corresponding with the second band of DMS is obtained.

$$\beta_{DMS} = \beta_{DMS\ exp} \text{ x correction factor} = 1.17 \text{ x } 0.78 = \mathbf{0.91} \qquad (7.10)$$

To estimate the error associated with this value, equation (7.8) is applied giving a value of 0.11. This gives the result of:

$$\beta_{\text{ for the second band of DMS}} = \mathbf{0.91 \pm 0.11} \qquad (7.11)$$

If this value is compared with the beta parameter for the second band of H_2S (β_{N2} second band = 1.12±0.05, [7]) it can be seen that the two values are similar.

The pressure reading on an ionization gauge is not the same for every gas at the same pressure, as each gas will have its own ionization efficiency in the electron impact source used in the ionization gauge [8, 9]. Also the pressure measured by the ion gauge, in the spectrometer in Southampton, will differ from that in the ionization cell (this will be explained in the next section).

- **7.2 Discussion.**

Accuracy and stability in the pressure measurement made during a reaction is also needed and this is the main problem of these studies. In Figure 7.2 it can be seen how the pressure measured by the ion gauge on the wall of the ionization chamber doesn't correspond to the pressure in the ionization cell. The normal pressure in the reaction cell used in these studies is around 1 x 10^{-4} torr; this corresponds to molar density of ~10^{12} molecules/cc. The pressure measured by the ion gauge is lower than that in the ionization cell by a factor of approximately 100 ([10]).

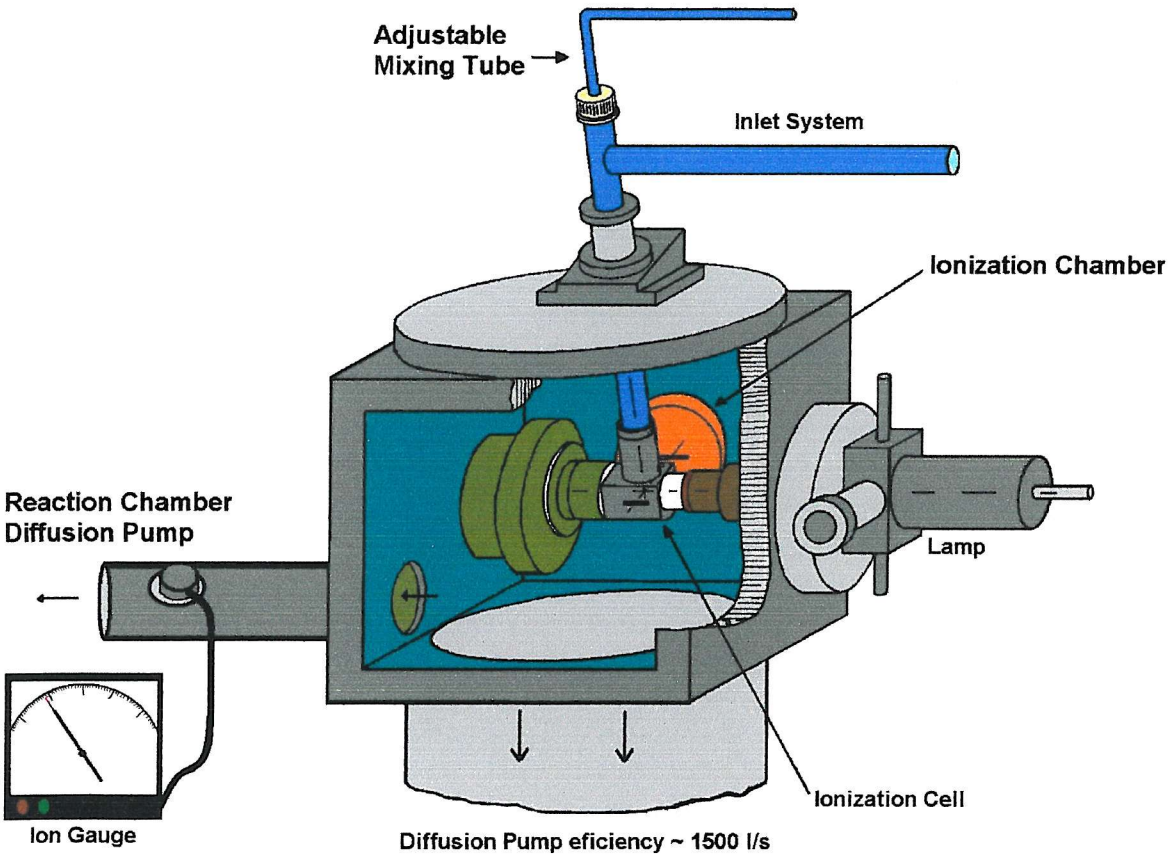

Figure 7.2: Schematic diagram of the spectrometer used in this work showing, the position where the pressure is measured.

In the experimental conditions used, the gas flow conditions deviate from ideal molecular flow by acquiring some viscous flow character. Hence pressure ratios measured at the ion-gauge (p_B/p_A, when a mixture of two gases is considered) do not correspond to those in the ionization cell (p_B^0/p_A^0).

To resolve the problem, a *correction factor* (**K**) must be use to relate these two ratios ([11]):

$$p_B/p_A = K\,(m_B/m_A)^{1/2}\;(p_B^0/p_A^0) \qquad (7.12)$$

This correction factor is needed because the mean speed of a gas is inversely proportional to the square root of its molecular weight [12].

$$\text{Mean speed} = (\,8kT/M\pi)^{1/2} \qquad (7.13)$$

- **7.3 Conclusion.**

In practice, conversion of photoelectron signals into relative partial pressures has not been achieved because of an error caused by the ion gauge. This error depends on the ionization potentials of the molecules present in the gases mixture.

Also, because the ionization gauge doesn't measure the pressure in the ionization cell but at some distance from it, a correction factor for the pressure measurements related to the molecular weight of each molecule should be included in order to obtain reliable results.

Both these problems must be allowed for if ionization gauge readings are to be used to estimate partial pressures in the reaction cell.

- **7.4 References.**

[1] J. L. Gardner and J. A. R. Samson.
J. of Electron Spectroscopy and Related Phenomena, **8** (1976) 469-474.

[2] Y. Achiba, T. Yamazaki and K. Kimura
J. of Electron Spectroscopy and Related Phenomena, **22** (1981) 187- 190.

[3] J. H. D. Eland
"Photoelectron Spectroscopy." Second Edition
Butterworths (1984)

[4] J. B. West, in
"Vacuum Ultraviolet Photoionization and Photodissociation of Molecules and Clusters"
C. Y. Ng (World Scientific, New Jersey, 1991), Chap. 8.

[5] W. H. Hancock and J. A. R. Sanson
J. of Electron Spectroscopy and Related Phenomena, **9** (1976) 211-216.

[6] J. R. Taylor
"An Introduction to error Analysis"

[7] S. Katsumata.
Chemical Physics Letters, **75** (1980), 196-198.

[8] *"Vacuum Equipment"* Catalogue
Edwards High Vacuum (1978).

[9] D. Hucknall
"Vacuum Technology and Applications"
Butterworth-Heinemann Ltd (1991) 139.

[10] Ph.D. Thesis, University of Southampton, 1989.
A.M. Ellis

[11] Y. Achiba, K. Kimura, N. Kakuta and K. Miyahara.
J. of Electron Spectroscopy and Related Phenomena, **28** (1982) 139-143.

[12] P. W. Atkins
"Physical Chemistry" Third Edition
Oxford University Press (1986)